ELSEVIER

Chemical Geology 222 (2005) 35–64

CHEMICAL GEOLOGY
INCLUDING
ISOTOPE GEOSCIENCE

www.elsevier.com/locate/chemgeo

An active amagmatic hydrothermal system: The Paralana hot springs, Northern Flinders Ranges, South Australia

Joël Brugger [a,b,*], Ngaire Long [c], D.C. McPhail [d], Ian Plimer [e]

[a] *School of Earth and Environmental Sciences, The University of Adelaide, Adelaide, South Australia;*
[b] *South Australian Museum, North Terrace, Adelaide, South Australia, Australia*
[c] *School of Geosciences, Monash University, Victoria 3800, Australia*
[d] *Cooperative Research Centre for Landscape Environments and Mineral Exploration (CRC LEME) and Department of Earth and Marine Sciences, The Australian National University, ACT 0200, Australia*
[e] *School of Earth Sciences, The University of Melbourne, Vic 3010, Australia*

Received 1 October 2004; received in revised form 26 May 2005; accepted 18 June 2005

Abstract

The Mesoproterozoic Mt. Painter Inlier (Northern Flinders Ranges, South Australia) is located in a zone of anomalously high heat flow attributed to high concentrations of radioactive elements in the Inlier. Paleozoic hydrothermal activity produced large volumes of uraniferous breccias and siliceous sinter, and secondary uranium deposits are mined in Tertiary sandstones east of the Inlier (Beverley mine). The Paralana hot springs (PHS) are the only remaining hot spring along the Paralana fault, the locus of long-standing hydrothermal activity, as shown by epithermal precious metal, Cu–Fe and Fe–U deposits. This study investigates the chemistry of the PHS water and other groundwaters in the Mt. Painter Inlier, aiming to constrain the primary source of the water and heat in PHS, and to explore the relationships between fossil ore deposits and modern groundwaters in the province.

PHS discharges 16 L/s of water at a temperature of 57 °C. The water is neutral (pH 7–8) and has total dissolved solids of 1144 mg/L, towards of the lower end of the range for nearby cold springs and groundwater bores (1000 to 3041 mg/L TDS). Fluorine (5 ppm), Mo (33 ppb), W (11 ppb), Cs (16 ppb) and Rb (200 ppb) concentrations are comparatively high in the spring water. $\delta^{18}O$ and δD values show that the PHS water is of meteoric origin, and $\delta^{13}C$ values of CO_2 (g) emanating from the springs and dissolved HCO_3^- suggest the carbon source is organic matter, e.g., soil or plants. Rn concentrations are very high at the springs (radiation of 10,952 Bq/m^3) implying a localized radiogenic source at shallow depth.

According to geothermometric calculations, the most recent water–rock interaction temperature is 95 ± 5 °C. High geothermal gradients, attributed to high concentrations of radiogenic elements, suggest that circulation depths between 1.4 and 2.4 km are required to produce this temperature. The PHS result from meteoric water circulating through hot rocks, and are the surface expression of a cyclic, low-temperature, non-volcanic hydrothermal system. Two possible sources of meteoric water for the springs have been identified: Mt. Painter Domain and a local Great Artesian Basin aquifer. The variability of the flow

* Corresponding author. South Australian Museum, North Terrace, Adelaide, South Australia, Australia.
E-mail address: Brugger.Joel@saugov.sa.gov.au (J. Brugger).

doi:10.1016/j.chemgeo.2005.06.007

rate, the low temperature of last equilibrium fluid–rock interaction, and the geochemistry of the springs indicate that the water is sourced from the Mt. Painter Domain.

The PHS contain negligible U (0.07 ppb), but some shallow groundwaters in the basement are enriched in U (300–600 ppb). Reactive transport modelling shows that these waters could produce Beverley-style mineralisation upon reaction with reduced carbon and/or sulphides. The PHS water, on the other hand, could produce upon cooling the jasperoidal mineralisation with traces of sulphides that outcrops along the Paralana fault. Hence, the chemistry of present-day groundwater may be related to that of the paleo-water responsible for major mineralisation events in the region, although particular circumstances affecting fluid flow and fluid chemistry (e.g., climate, tectonism, or magmatism) must have been instrumental in the formation of the major deposits.

Keywords: Water chemistry; Epithermal system; Hot springs; Uranium deposits; Geochemical numerical modelling; Mt. Painter Domain, Northern Flinders Ranges, South Australia

1. Introduction

Hydrothermal systems are found in a wide variety of geological environments, e.g., seafloor hydrothermal vents, sedimentary basins, epithermal to magmatic-hydrothermal ore-forming environments; these environments determine the chemical composition and flow path of the fluids (Barnes and Rose, 1998). Hydrothermal systems have been extensively studied for their potential as geothermal reservoirs for power generation (e.g., Huttrer, 2001), to gain a greater understanding of the processes involved in hydrothermal ore transport and deposition (e.g., Henley, 1985), or as analogues for modelling fluid flow and mass transport around high-level radioactive waste deposits (e.g., Druschel and Rosenberg, 2001). In order to understand hydrothermal systems, ultimately we need to understand the effects of fluid flow, heat flow, structure and lithology as well as the geochemical reactions between fluids, rocks and vapours. These factors are interdependent and control the overall geometry and the physical and geochemical behaviour of large-scale flow of hydrothermal fluids in the crust (e.g., Heinrich et al., 1996).

The Paralana hot springs (PHS) are one of several springs in the Northern Flinders Ranges of South Australia, but they are enigmatic because they are the only hot springs in the area (Mawson, 1927). They represent present-day geothermal activity, presumably because of high heat flow associated with the naturally radioactive rocks in the Mt. Painter Inlier, which underlies the Northern Flinders ranges (Coats and Blissett, 1971; Mawson, 1927). Because they are not associated with any active or quiescent volcanism, the PHS provide an opportunity to investigate the consequences of amagmatic heat sources capable of driving a hydrothermal system over a long period of time, perhaps a billion years or more (Neumann et al., 2000). This is relevant for understanding the fluid and geological evolution in such terrains, and their consequences in terms of ore deposits and geothermal energy.

There are many occurrences of hydrothermal mineralisation in the Northern Flinders Ranges and surrounding region, including massive Palaeozoic iron oxide ± U, Mo-bearing siliceous sinters, epithermal Cu ± Au ± Bi, V, As, U and fault-bound jasperoids (Coats and Blissett, 1971). They testify to previous large-scale hydrothermal activity in the Northern Flinders Ranges and surrounding region. 15 km east of the PHS, the Beverley mine produces uranium from secondary deposits in Tertiary sands underlying Lake Frome (Walker, 1999). That uranium may have been derived from the Mount Painter Domain. The region is also actively explored for the production of geothermal energy (e.g., Hillis et al., 2004), and the PHS provides a natural laboratory to study fluid flow, heat transfer and reactive transport that will help in developing geothermal energy resources, e.g., the engineering of geothermal plants.

Because the PHS offer a permanent water source in an arid environment, they support a rich ecosystem. The microbiological association in the PHS has been studied as an analogue for early life and microbial adaptation to extreme temperatures and radioactivity levels (e.g., Anitori et al., 2002). The PHS are also culturally important, and have a special significance for aboriginal people (Sprigg, 1984). The radioactive springs were briefly used as a medical spa in the 1926-1928, but their remoteness made this attempt uneconomical at the time (Sprigg, 1984). The PHS

were listed in 1980 as a Geological Monument in the Register of the National Heritage in recognition of their geological and cultural significance.

Despite their uniqueness and potential for greater understanding of the regional hydrogeology, heat flow and economic geology, the PHS remain poorly studied. Their radioactivity attracted the interest of pioneer researchers (Grant, 1938; Mawson, 1927). Mawson (1927) was the first to suggest that the high U–Th content of the host rocks was driving hydrothermal circulation in the Mt. Painter Inlier. Grant (1938) measured the radioactivity of the water and associated gas, showing that the radioactivity is due to high Rn contents in the gas phase, which also contains traces of radiogenic He (i.e., 560 ppm). Both authors provided analyses of the main anions and cations in the PHS water. More recent analyses were conducted as part of a regional hydrogeological survey as part of the environmental impact study for the Beverley in situ leaching uranium mine (Heathgate Resources, 1998). McKelson (2000) studied the local geology around the PHS.

The general aim of this study is to understand the reasons for the presence of the PHS, and to understand better the consequences of long-lived high heat flow geological terrains. More specific aims are to:

- Use the geochemistry of the discharging water and gas from the PHS to understand the sources and pathways of the water and its dissolved constituents;
- Understand the processes that affect the water composition in the PHS, e.g., water–rock interaction, fluid mixing, cooling;
- Infer the mineralising potential of the groundwater in the PHS and other springs and bores in the Mt. Painter Domain; and
- Use the results of present day mineralising potential to understand the formation of fossil mineralisation and epithermal features in the area.

2. Geological and hydrogeological settings of the PHS

2.1. Location, geologic and tectonic settings

Mt. Painter and Mt. Babbage Inliers, collectively known as the Mt. Painter Domain (MPD), are part of the Northern Flinders Ranges in South Australia (Fig. 1a,b; Drexel et al., 1993). The MPD consists of Palaeo(?)- to Meso–Proterozoic granites, gneisses and metasediments that are overlain by Neoproterozoic to Cambrian sediments of the Adelaide Geosyncline (Coats and Blissett, 1971; Preiss, 1990; Fig. 1a,b). Both basement and cover have been deformed during the Cambro–Ordovician Delamerian orogeny, with shortening of approximately10–20% (Paul et al., 1999). The MPD is bounded to the east by the Paralana fault system, and thrusts eastward over the Mesozoic and Tertiary sediments of the Lake Frome embayment (Coats and Blissett, 1971).

The inliers are best known for the abundance of high heat-producing granites in the basement (Drexel and Major, 1990; Neumann et al., 2000), and their proposed effects on thermal and structural events during the Delamerian orogeny (McLaren et al., 2002; Mildren and Sandiford, 1995; Paul et al., 1999; Sandiford et al., 1998b). Metamorphism during the Delamerian orogeny did not exceed greenschist facies conditions over most of the Flinders Ranges (Preiss, 1989); however, there is a high-grade metamorphic overprint that is restricted to the Mt. Painter Inlier and to a narrow halo (<5 km) in the surrounding Adelaidean sediments (Sandiford et al., 1998b). The metamorphic grade increases markedly from very low grade to lower amphibolite facies as the contact with the Mt. Painter Inlier is approached. This unusual metamorphism has been attributed to the extremely high concentration of heat-producing elements in the Inlier (Sandiford et al., 1998b), although other authors have suggested that mantle heat in the form of large granite body (British Empire Granite) was involved (Elburg et al., 2003).

The Lake Frome embayment lies to the east of the Northern Flinders Ranges, on the southern margin of the Late Triassic to Late Cretaceous Great Artesian Basin (GAB; Cox and Barron, 1998; Fig. 2b). The sediments in the embayment contain both marine (stratigraphic middle) and fluviatile and lacustrine (top and bottom) deposits. The Tertiary sediments are characterised by fluvio-lacustrine deposits capped by silcrete and duricrust that resulted from deep chemical weathering (Fig. 3). Tertiary and more recent tectonic movements established the main present topographic features of the MPD, creating the surrounding Lake Frome, Lake Eyre and Lake Torrens basins (Idnurm and Heinrich, 1993; Ludbrook, 1969; Foster et al., 1994). This tectonism caused the uplift and erosion

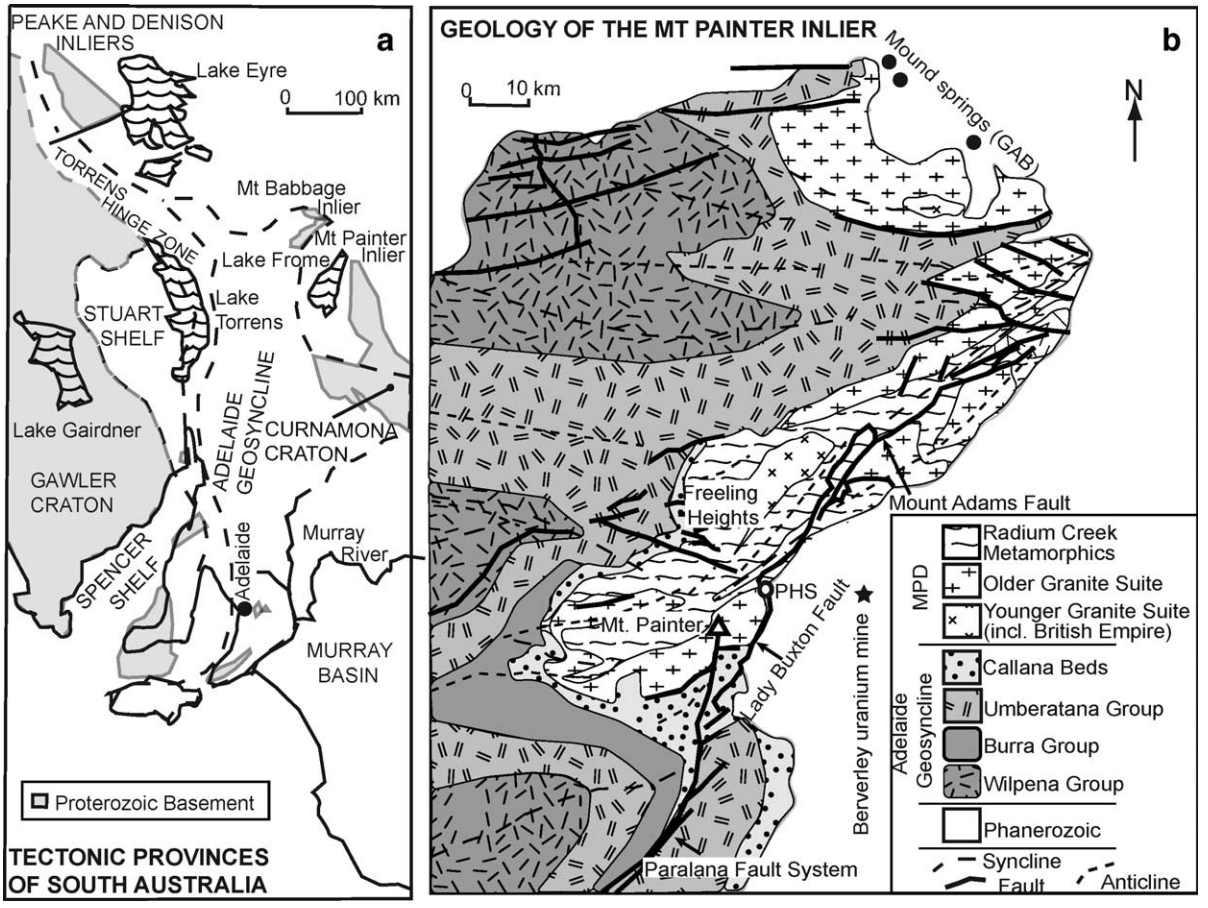

Fig. 1. Geological context of the study area: (a) regional geological context and (b) schematic geological and tectonic map of the Mt. Painter Domain. See Fig. 2 for location within Australia.

of the MPD along the Paralana fault system and deformed Mesozoic sediments in the Eromanga basin.

2.2. Paralana fault system

The Paralana fault system is a major structural discontinuity that separates the Adelaide Geosyncline from the Curnamona province (Sandiford et al., 1998b; Fig. 1). The system has been intermittently active since the Middle Proterozoic (Foster et al., 1994). The uplift of the MPD along the Paralana fault system is attributed to reverse and strike-slip components (Preiss, 1993), although subsequent reverse-thrust, oblique-slip and normal movements have been reported (Foster et al., 1994; Teale, 1993). Minor tremors indicate that the Paralana fault system is still active today, currently with reverse movement (Sprigg, 1984). This uplift has shed sediments to the east (Frome Embayment) and west (Eyre basin), and affects local fluvial and groundwater flow (Coats and Blissett, 1971).

Numerous northeasterly trending splays branch off the Paralana fault, including the Lady Buxton Fault (Fig. 1b; Coats and Blissett, 1971). The PHS are located on this fault, in a dilational zone where there is a right angle deflection in the trend of the Lady Buxton Fault (Fig. 1b). To the north, an easterly dipping upthrust structure known as the Mt. Adams Fault truncates the Lady Buxton Fault (Coats and Blissett, 1971). Directly west of the PHS a series of faults that trend west–northwest and west–southwest (Mt. Saturday radial system) disrupt the crystalline basement and

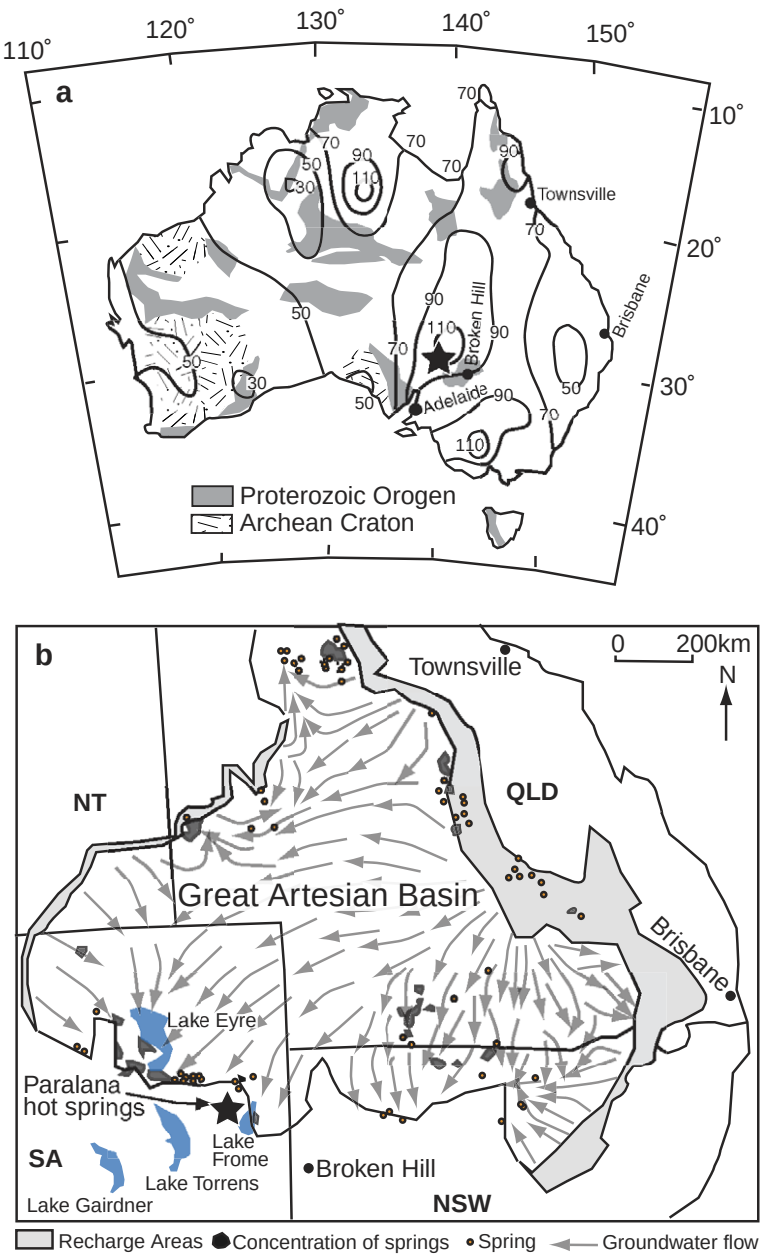

Fig. 2. Geographical, heat flow, and hydrological context of the study area. (a) Location of the study area (star) in Australia, and with respect of the surface heat flow (modified after Neumann et al., 2000). (b) Location of the study area on the SW border of the Great Artesian Basin (GAB). Arrows indicate flow path of the waters from the recharge areas (in grey) to the discharge areas. Modified after Habermehl (1980).

Adelaidean sediments (Coats and Blissett, 1971). A west–northwest trending lineament also intersects the Paralana fault at the PHS, based on LANDSAT images (Stamoulis et al., 1999), and may be a continuation of the Mt. Saturday system.

2.3. Climate and regional aquifers

The climate of the region is arid with marked diurnal and seasonal temperature extremes (average daily extreme of temperatures of 17–34 °C in summer

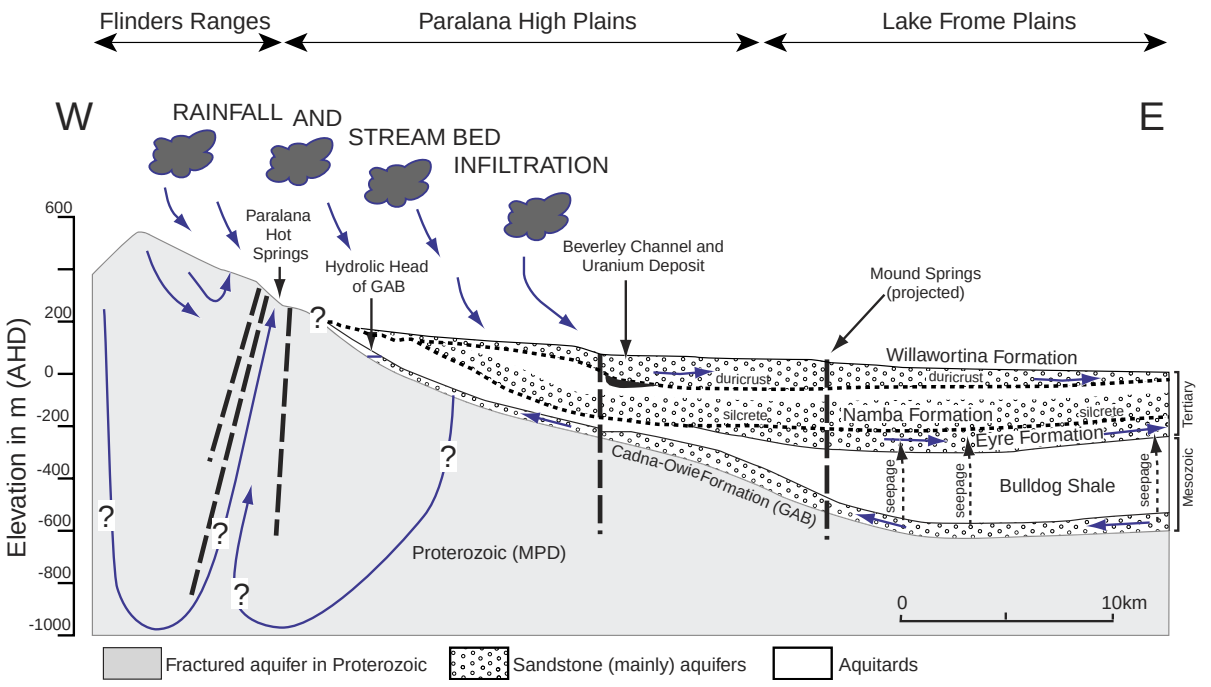

Fig. 3. Schematic cross-section from the Mt. Painter Domain to the Lake Frome Embayment, showing the different aquifers and their connections. Modified from Heathgate Resources (1998).

and 2–17 °C in winter; Sprigg, 1984). The area is drought-prone and rainfall at local stations is erratic and unpredictable with the arid climate interrupted by flash flooding from infrequent thunderstorms. The average annual rainfall between 1874 and 1983 was 20.3 mm, with an extreme of 1270 mm in 1974 (Sprigg, 1984).

There are five aquifer systems in and around the MPD (Heathgate Resources, 1998; Fig. 3): (1) fractured high-grade metamorphic rocks in the MPD (Proterozoic); (2) Cadna-Owie Formation (Cretaceous sandstone; GAB aquifer); (3) Eyre Formation (blanket and palaeochannel Tertiary sands); (4) Namba Formation aquifer (uncemented Tertiary sand, clay and silt); (5) Willawortina Formation and younger aquifers (Tertiary and Quaternary conglomerates and poorly sorted sands in clays, and aquifers in younger stream sediments which incise into the Willawortina Formation). The Cadna-Owie, Namba, Eyre and Willawortina Formations are all in the GAB to the east of the MPD, where the elevation drops from up to 900 m in the North Flinders Ranges to sea level in the Lake Frome plains.

The MPD comprises fractured rock aquifers with the highest yield next to faults, where most springs occur (Kerr, 1966). Recharge is limited to direct infiltration from rainfall, and the water table, while variable, generally follows topography, i.e., highest elevation in the eastern part of the Mt. Painter Inlier and a sharp decrease in elevation further east to the Lake Frome plains. The water level in wells and bores located at higher elevations near Mt. Painter show that the water table in the MPD lies about 9 m below the surface. Groundwater from the MPD discharges into ephemeral creeks and along the range front at springs, one of which Heathgate Resources (1998) suggested is the PHS.

The GAB covers ~22% of Australia (Fig. 2b). Recharge areas are located on the Eastern and Western flancs, and the bulk of the discharge occurs on the Southern flank (Fig. 2b). The Lake Frome Embayment SE of the PHS acts as a discharge area for the GAB aquifer through the Cadna-Owie Formation (continental sandstones). The formation has a present-day hydraulic head of approximately 90 m AHD and a temperature of 50 °C underneath the

Beverley deposit (Heathgate Resources, 1998). Water discharges from the GAB aquifer system through diffuse upwards leakage, and from point sources such as mound springs. Mound springs build up from the deposition of particles transported from the underlying aquifers and confining beds, cemented by precipitated carbonates (travertine/calcrete), gypsum and organic silt (Sheard and Smith, 1995). Mound springs in the GAB have low discharge rates ranging from <1 to 150 L/s (Habermehl, 1980). Around the MPD, mound springs are located to the north of the Mt. Babbage Inlier and on the eastern edge of Lake Frome (Figs. 1b and 2b). In general, groundwater in the Lake Frome area is recharged from the GAB to the north-east, indicating that local discharge has travelled 800 to 900 km through GAB aquifers (Habermehl, 1980).

The clay-capped Namba Formation confines the Eyre Formation. Both formations discharge groundwater into Lake Frome, where evaporation is the principal discharge mechanism (Heathgate Resources, 1998). Recharge is from the MPD through subsurface flow and surface runoff. The Eyre Formation is also recharged via upwards seepage from the Cadna-Owie Formation (Fig. 3). The Willawortina Formation shows a similar recharge pattern, i.e., from the west, with recharge primarily from direct infiltration and surface runoff (Fig. 3).

2.4. Regional heat flow

Neumann et al. (2000) identified a zone of anomalously high surface heat flow, known as the South Australian heat flow anomaly (SAHFA), centred on the western margin of the Adelaide Geosyncline, and extending to the Gawler Craton and Stuart Shelf in the west and the Curnamona province in the east (Figs. 1a, 2a). Within this zone, the highest surface heat flow was measured in the MPD at 126×10^{-3} W m^{-2} (Cull, 1982; Sandiford et al., 1998a), approximately double the global mean for Proterozoic rocks (Pollack et al., 1993). Sandiford et al. (1998a) estimated the mean heat production of the MPD to be 9.9×10^{-3} W m^{-3}, four times the heat production for average granites (2.5×10^{-3} W m^{-3}). Such values have been attributed to high U and Th concentrations in the local granites (Sandiford et al., 1998a). The thermal regime of the MPD may also be significantly affected by its recent uplift (Neumann et al., 2000). PHS are the only documented example of hydrothermal activity within the SAHFA.

2.5. Fossil hydrothermal deposits

The MPD and the surrounding sediments contain a large variety of ore deposits and occurrences (Coats and Blissett, 1971), which reflect a long history of hydrothermal circulation in and around the inliers. Epithermal deposits in particular are of interest because they document shallow fossil hydrothermal systems. There are two types of epithermal deposits in the MPD: (i) Fault-bound deposits occur along the Paralana and associated faults; they are characterised by jasperoids and laminated crack-seal quartz veins showing multistage brecciation and chalcedony flooding and contain elevated concentrations of Au, As, Cu, Se, Te, U, Bi and V (Collier, 2000; McKelson, 2000). Apatite-fission track thermochronology suggests that pervasive hot springs activity took place along the Paralana fault system in mid-Tertiary, ending with a subsequent stage of uplift (Foster et al., 1994; Mitchell et al., 2002). (ii) Complex quartz–hematite veins at Mt. Gee and Mt. Painter (Fig. 1b) represent a shallow epithermal system and laminated quartz–hematite sinter on the summit of Mt. Painter probably is its surface expression (Coats and Blissett, 1971; Drexel and Major, 1987, 1990). In the epithermal veins, fluorite, barite and bladed calcite are commonly totally silicified. A late stage of quartz veins contains locally abundant acicular laumontite crystals, which often grew into cavities that were over a metre in size, and were overgrown by radial quartz before being dissolved ("nailhole quartz"; Coats and Blissett, 1971). Open spaces were filled with hydrothermal sediments consisting of silicified hematite. The hematite ore contains elevated REE (mainly as monazite-(Ce)), U (torbernite in cavities) and Mo concentrations, and minor gold and roscoelite are reported from drill core. This system is associated with high-temperature hematite breccia enriched in U, REE ± Cu, Mo, Nb (Drexel and Major, 1987, 1990). It is Palaeozoic, although an accurate age remains contentious (Permo-Carboniferous, Idnurm and Heinrich, 1993; Devonian, Elburg et al., 2003).

The Willawortina formation, east of the Paralana fault system, hosts sedimentary uranium deposits,

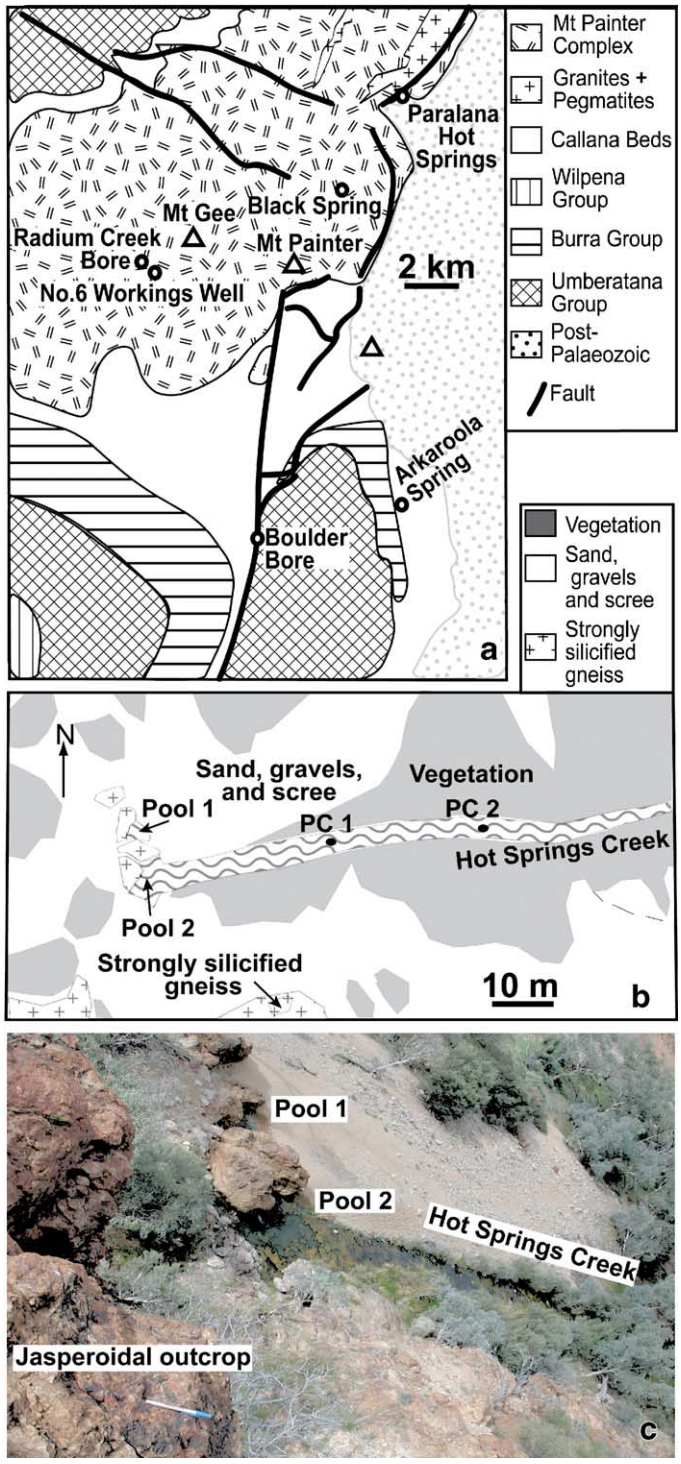

Fig. 4. Location of water samples, (a) regional samples; (b) samples from the Paralana Hot Springs; (c) photograph of the Paralana Hot Springs, showing the two pools and the start of Hot Springs Creek.

which are presently mined by in situ leaching at the Beverley mine (Howles, 2000). The deposits consist mainly of coffinite, and are located in Tertiary channels. It is assumed that the uranium in these deposits was leached from the U-rich rocks of the MPD.

3. Local geology and site characteristics

The local geology and site maps of the PHS and other springs are shown in Fig. 4. The PHS are located on the Paralana fault. The MPD around the springs consists of granitic gneisses that are highly hydrothermally altered (McKelson, 2000). The PHS consist of two pools that are drained by the Hot Springs Creek (Fig. 4b,c). The springs appear to discharge mainly or solely into Pool 1, which during our two sampling trips in 2001 contained clear water over a gravel bed and no observable biota. Streams of bubbles escaped intermittently from the bottom of the pool. Pool 1 had a surface area of approximately 9 m^2 and a depth of approximately 80 cm. Pool 2 was bigger, approximately 80 m^2 and 1–1.5 m deep, and bacterial mats covered its surface and bottom, similarly to the observation of Mawson (1927). The temperature of the water in Pool 1 was 56.8 °C, compared with previous measurements of 62.2 (Mawson, 1927), 60 (Grant, 1938) and 63 °C (Anitori et al., 2002). The temperature of Pool 2 was 40.2 °C. Discharge of the springs was not measured directly; however, stream flow was estimated in Hot Springs Creek, approximately 50 m downstream of Pool 2. Based on measured surface water velocity and cross sectional area of the creek, stream flow was estimated to be 16 ± 2 L/s (~60,000 L/h). Mawson (1927) estimated the flow to be in excess of 4500 L/h.

4. Methods

Water was sampled from several springs and bores in the area and several sites at the PHS (see locations in Fig. 4b) in two separate field trips: April and July 2001. In addition, gas, sediment and rock were sampled at the PHS. Water was sampled from Pool 1, Pool 2 and in Hot Springs Creek approximately 40 m (PC 1) and 80 m (PC 2) downstream of Pool 2.

4.1. Water sampling and analysis

Four water samples were taken at each site: one untreated for alkalinity and acidity measurements; one filtered for anion analysis; one filtered for stable isotope analysis; and one filtered and acidified for cation and trace element analysis. Water samples were collected in new, but otherwise unprepared 1 L HDPE bottles, which were rinsed twice with water from the sample site. For bores and wells, a nylon bailer attached to a nylon rope was first rinsed with sample water and then used to collect samples, which were emptied into a wide-mouth HDPE bottle before filtration or acidification. An extra sample from the bailer was emptied into a plastic cup for field measurements. Requisite samples were filtered though 0.45 μm cellulose nitrate filters in a plastic vacuum filtration apparatus that was acid washed before use in the field, rinsed with double deionised water between samples and rinsed with a small amount of filtered sample before collecting samples for analysis. Cation and trace element samples were acidified with 1 M reagent grade nitric acid to approximately 4 vol.% nitric acid. All sample bottles were stored upright, on ice and in the dark for transport and then refrigerated at 4 °C until analysis.

Temperature, pH, Eh, electrical conductivity (EC) and dissolved oxygen (DO) were measured on site, either in situ or as soon as possible after retrieving samples. Orion meters and electrodes were used after calibration with Orion standards (pH 4 and 7 buffers) or checking against Orion or recently prepared standards (i.e., 692 ppm NaCl for EC, Zobell's solution for Eh). DO was measured using a Hach DO Test kit. Uncertainties were estimated by measuring standards and 4 replicates of samples: $T \pm 0.5$ °C; pH ± 0.01; Eh ± 10 mV; EC ± 20 μS/cm; and DO ± 0.2 mg/L.

Alkalinity and acidity were measured within 12 h of sampling. Alkalinity was measured using Standard Method 403 (Eaton et al., 1995): 100 mL samples were titrated with 0.01006 m sulphuric acid and pH was monitored. The alkalinity was calculated using the inflection point of the curves. Acidity was measured similarly using Method 402 (Eaton et al., 1995), where 100 mL samples were titrated with 0.01042 m NaOH. Uncertainty in both alkalinity and acidity is estimated to be $\pm 10\%$, based on replicate analyses. The uncertainty is higher for Arkaroola Spring and

Number 6 Workings Well because high contents of organic matter resulted in poorly defined inflection points.

The element geochemistry of the water samples was measured using a combination of ICP-AES, ICP-MS and ion chromatography. Major cations and heavy metals were analysed by ICP-AES at ALS Environmental in their Melbourne laboratory except lithium in their Sydney laboratory. Duplicate samples indicated reproducibility was ±3 wt.%, which we use as an estimate of the uncertainty. Acidified, double-deionised water was submitted as a blank and elements were at or below their detection limits. Trace elements were analysed by a HR-ICP-MS fitted with a platinum guard electrode in the geochemistry laboratories at Monash University. The reproducibility of samples and standards was within ±5% for most trace elements, and ±10 wt.% for elements at concentrations near the detection limit. Ion chromatography (IC) in the geochemistry laboratories at Monash University was used to measure anion concentrations. Estimated uncertainty is ±3 wt.% for fluoride, chloride, bromide, phosphate and sulphate and ±9 wt.% for nitrate. We also checked the accuracy of our measured water compositions by calculating charge balances, and they are typically smaller than 5.5% (Table 1), indicating that our analyses were within that error for major elements. The exception of No. 6 Workings Well (+25%; Table 1) is probably because that sample was observably rich in organic matter, where the positive imbalance could have resulted because the alkalinity titration was not accurate and organic acid concentrations were not measured and hence are not included in the charge balance calculations. The charge balances for other samples are systematically negative, which probably indicates a small systematic error in the Na^+, Cl^- and/or SO_4^{2-} concentrations, as they have the highest concentrations.

Oxygen, hydrogen and carbon isotopic ratios in waters and carbon isotopic ratios of the carbon dioxide in the gas were measured using a Finnigan MAT 252 mass spectrometer at Monash University. Oxygen was equilibrated with carbon dioxide at 25 °C for 24 h before analysis. Hydrogen was analysed via reaction with chromium ($2Cr+3H_2O \rightarrow Cr_2O_3+3H_2$) at 850 °C using the automated MAT H/Device. Carbon was analysed as carbon dioxide after reaction with phosphoric acid.

4.2. Gas sampling and analysis

Gas samples were collected by displacement into 250 mL Schott bottles, which were filled with spring water, submerged, inverted and directed over gas streams. Gas bubbles displaced the water and the top was screwed on the bottles while still submerged, leaving a small amount of water in the bottle to help seal the cap and minimise any gas leak into or out of the bottle. The bottles were stored inverted and in the dark until analysis. Charcoal traps were placed at the four sampling sites—Pool 1, Pool 2, PC1 and PC2—to collect radon, and were exposed to the atmosphere for 8 h. The vials were then kept upright and in the dark for transport to the Australian Nuclear Science and Technology Organisation (ANSTO) in Sydney for analysis. Gas samples were collected on two separate occasions, i.e., during the April and July field trips. In April, four gas samples were collected and subsequently analysed for their major constituents. In July, ten samples were collected of which four were analysed for their major constituents and six were used to analyse the carbon and oxygen isotopic ratios within the carbon dioxide. Two samples taken in April were discarded due to contamination by atmospheric gas.

Gas samples were analysed at ANSTO by gas chromatography-thermal conductivity detection (GC-TCD) with an MTI P-200 dual channel micro-TCD gas chromatograph, containing a molecular sieve column and a Poraplot-U column used for detection of gases above 5 ppm. The molecular sieve column enables the detection of He, H_2, O_2, N_2, Ar and CH_4, while the Poraplot-U column enables O_2, N_2, CH_4 and CO_2 to be detected. N_2 was used as the carrier gas for detection of He and H_2, and He for detection of O_2, N_2, CH_4 and CO_2. Samples were analysed in duplicate and a blank was run between samples. The concentrations were calculated from the peak area of each gas in the chromatograms, and the results normalised to 100%. Carbon and oxygen isotope ratios of the CO_2 in the gas were analysed as above, after purifying the CO_2 by twice freezing and separating non-condensable gases.

4.3. Rock sampling and analysis

Rock was sampled from an outcrop adjacent to Pool 1 (Fig. 4b) by using a hammer to break off

Table 1
Field measurements and major ions in waters from the Paralana Hot Springs and Mt. Painter Inlier

	Pool 1				Pool 2	PC 1	PC 2	Black Spring		Boulder Bore	No. 6 Workings Well	Radium Creek Bore	Arkaroola Spring
	This study	Mawson (1927)	Grant (1938)	Heathgate Res. (1998)				This Study	Mawson (1927)				
$pH_{Temperature}$	6.40				7.05	6.87	6.82	7.86		7.47	7.85	6.92	8.43
Temperature (°C)	56.8	62	60		46.6	45	40.2	24.4		25.8	22.7	23.7	28.3
EC (μ S/cm)	2130			1800	2040	1970	1940	2470		1660	2880	1410	1100
Eh (mV)	22				59		−12	−44		−17	−100.4	−23	−24.1
DO (mg/L)	1.5				6	4	4				0.6	3	
Log fO_2 (g) (DO)[1]	−1.28				−0.71	−0.89	−0.92				−1.86	−1.15	
Log fO_2(g) (Eh)[2]	−47.9				−45.4		−52.4	−54.8		−54.2	−59.2	−57.4	−50.1
HCO_2^-(mg/L)[3]	258	160	170	227	258	258	258	602	172	399	1217	590	418
CO_2 (aq) (mg/L)[4]	31.6			57	20.6	24.3	18.3	10.1		17.0	4.6	32.1	
TDS (EC) (mg/L)[5]	1420			1100	1360	1313	1293	1647		1107	1920	940	733
TDS (Calc) (mg/L)[6]	1144	1297	1280		1146	1151	1158	1819	1479	1475	3041	1484	1000
Charge Balance (%)	−0.15				−1.27	−1.46	−0.98	−3.15		−5.43	23.61	−3.42	−1.05
Major cations													
Na^+ (ppm)	272	368	333	300	273	274	297	428	435	226	679	209	160
K^+ (ppm)	23	96	37	24	22	22	23	29	45	26	16	7	18
Ca^{2+} (ppm)	42	56	59	46	41	41	40	75	60	50	186	105	51
Mg^{2+} (ppm)	15	3	27	16	15	15	15	19	15	68	181	61	48
Major anions													
F^- (ppm)	4.9			4.5	4.9	4.9	4.9			1.3	1.0	3.7	0.3
Cl^- (ppm)	310	391	398	310	312	314	316	526	522	249	249	276	218
Br^- (ppm)	0.76				0.77	0.77	0.77	1.26		0.96	0.96	0.94	0.66
NO_3^- (ppm)	0.34				0.10	0.16	0.09	0.17		155	199	45.7	0.13
SO_4^{2-} (ppm)	136	183	178	66	136	138	137	76	173	215	215	126	57

[1] Calculated from dissolved oxygen; [2] calculated from Eh; [3] calculated from alkalinity titration; [4] calculated from acidity titration; [5] calculated from EC; [6] sum of element concentrations.

samples, which were stored and transported in plastic sample bags. Thin sections were prepared and analysed by conventional petrographic methods, using both transmitted and reflected light, and by scanning electron microscopy equipped with an energy dispersive X-ray spectrometer for qualitative elemental analysis.

5. Results

The results of water geochemistry are listed in Tables 1 and 2 and gas geochemistry in Table 3. We focus on the results of the PHS, and compare them with the results of the other spring, bore and well waters. Note that the other waters may not represent subsurface conditions because we do not know the discharge rates of the springs and we were not able to purge the Boulder and Radium Creek bores (both were capped) or the No. 6 Workings well (open).

5.1. Water geochemistry

The temperature of the PHS water decreased from 56.8 °C in Pool 1 to 40.2 °C at PC 2 (Table 1). The other springs in the area had temperatures of 24.4 (Black Spring) and 28.3 °C (Arkaroola Spring), which reflect ambient temperature. The temperatures of the No. 6 Workings Well and Radium Creek bore are unlikely to represent groundwater temperature because we could not purge the wells during our field work and the samples were heated during measurement. Electrical conductivities of water at the PHS decreased downstream from 2130 μS/cm in Pool 1 to 1940 μS/cm at PC 2, a result of decreasing temperature as the TDS values calculated as a sum of measured element concentrations are approximately constant (Table 1). Black Spring and the No.6 Working Well had the highest EC and Boulder Bore, Radium Creek Bore (RC) and Arkaroola Springs all have significantly lower values and lower TDS values (Table 1).

The $pH_{56.8\ ^\circ C}$ of Pool 1 of the PHS was 6.40, compared to $pH_{24.4\ ^\circ C}=7.86$ for Black Spring and $pH_{28.3\ ^\circ C}=8.43$ for Arkaroola Spring (Table 1). The pH of the PHS water increased from $pH_{57\ ^\circ C}=6.40$ in Pool 1 to $pH_{47\ ^\circ C}=7.05$ in Pool 2 and then decreased to $pH_{45\ ^\circ C}=6.87$ at PC1 and $pH_{40\ ^\circ C}=6.82$ at PC2. The small differences in pH are due to changes in temperature and probably higher CO_2(g) input into Pool 1 (see gas analyses below) and variable amounts of biota, i.e., no biota were observed in Pool 1 and abundant biota were observed in Pool 2 and downstream.

Redox was measured using dissolved oxygen (DO) and Eh. In order to compare results from different measurements, we calculated $\log f_{O2(g)}$ from both DO and Eh (e.g., Anderson and Crerar, 1993, p. 503) using Geochemist's Workbench (Bethke, 1998). Log $f_{O2(g)}$ values calculated from DO (Table 1) show that the PHS waters were slightly undersaturated with respect to atmospheric oxygen, i.e., calculated values range from −1.3 to −0.71, compared with −0.70 for atmospheric pressure of 0.2 bars. Although we attempted to avoid interaction with atmosphere during sampling and measurement, we consider our DO values to be maximum values. The $\log f_{O2(g)}$ values calculated from Eh range from −45 to −52, much lower than those calculated from DO. The low concentrations of metals in the water (Table 2) probably prevented accurate measurement of Eh (e.g., Drever, 1997); however, the values are consistent with the observed mineralogy of gypsum and pyrite (see below) and the faint smell of H_2S around the springs, which suggests redox conditions near the sulphide–sulphate boundary (Fig. 5). The DO measurements and the Eh values may both be accurate and just reflect redox disequilibrium. The higher DO values in Pool 2 and Hot Springs Creek waters are likely a result of photosynthesis (e.g., Drever, 1997) and/or they are closer to saturation with respect to atmospheric oxygen. The other springs, well and bore waters in the area show similar differences between DO and Eh.

In the PHS and Hot Springs Creek, HCO_3^- concentrations, calculated from alkalinity titrations, are the same, i.e., 258 mg/L (Table 1). Dissolved CO_2, calculated from acidity titrations, decreased from Pool 1 to Pool 2, increased and then decreased at PC 1 and PC2, respectively. The higher concentration of dissolved CO_2 in Pool 1 reflects the CO_2(g) in the gas streams (Table 3). The decrease in dissolved CO_2 to Pool 2 could be a result of degassing, but the subsequent increase in dissolved CO_2 further downstream and the observation that DO is highest in Pool 2 suggest that photosynthesis is affecting the water composition in Pool 2 ($CO_2 \rightarrow C_{biological} + O_2$; e.g.,

Drever, 1997). The other springs were mostly alkaline, with HCO_3^- concentrations of 602 mg/L for Black Spring and 418 mg/L for Arkaroola Spring (Table 1). Boulder and Radium Creek bores had 399 and 590 mg/L, respectively. The No. 6 Workings well had a higher concentration of 1217 mg/L HCO_3^-, probably a result of rotting biologic matter present in the well at the time. Other bores and surface waters had lower dissolved CO_2 concentrations (5–17 mg/L) with the exception of Radium Creek bore which contained 32 mg/L (Table 1).

5.2. Major elements

Concentrations of dissolved major cations and anions do not vary from Pool 1 to PC 2 at the PHS, aside from small changes in nitrate (Table 1; Fig. 6). The concentrations of Na and K of the PHS fall within the range of the other waters in this study; however, the PHS have lower Mg and Ca concentrations (Table 1). The chloride concentration of the PHS is higher than the other waters, except for Black Spring, and the sulphate concentration of the PHS is higher than the other spring waters but lower than the Boulder Bore and No. 6 Working Well (Table 1). Compared to the PHS, nitrate concentrations are high in Boulder and Radium Creek bores and the No. 6 Working Well, which may be a result of increased biomatter and biotic activity. Fluoride concentration in the PHS was higher than in the other waters, whereas bromide is lower than in most of the other waters (Table 1). Concentrations of major elements in PHS water measured in this study and those reported by previous studies are similar, indicating there has been little change in water chemistry over the intervening 74 years (Table 1, Pool 1).

Two groups emerge when major elemental compositions are plotted on a Piper diagram (Fig. 6). PHS and Black Spring waters are dominated by Na+K and carbonate, and all other waters have higher percentages of Mg and Ca. These groupings suggest different flow paths, if not different sources for the two groups. The results for the No.6 Working Well are slightly different from the rest of the group according to its bicarbonate concentration, which may be unreliable because high concentrations of biogenic carbon resulted in poorly defined inflection point during titration. Cl/Br ratios also allow to discriminate among these two groups: PHS (408) and Black Spring (417) have significantly higher Cl/Br ratios than the other sampled regional springs (259–330), which scatter along the sea-water value of 289 (Drever, 1997). Values of 550–690 have been reported for waters in the Southern part of the GAB (Herczeg et al., 1991).

Compared to waters from the Lake Frome plains down hydraulic gradient from Mt. Painter Inlier to the east of the Paralana fault System, PHS and Black Spring show the greatest similarity to waters from the Willawortina Formation (Fig. 6). The cation composition of PHS and Black Spring plots between the fields defined by the other Mt. Painter Inlier groundwaters and that of the Willawortina formation waters (Fig. 6). In general (Heathgate Resources, 1998), Willawortina waters ($n=39$) are more saline (EC 1000–20,000 mg/L) than waters from the fractured aquifers in the Mt. Painter Inlier ($n=36$; EC 600–3000 mg/L) and the GAB ($n=4$; EC 1605–2100 mg/L). Note that the Willawortina waters are most saline at shallow depth (EC<3500 mg/L at depths >50 m); this reflects evaporation and links with the Lake Frome salt lake. The Willawortina waters are thought to be recharged by groundwater circulating through the Mt. Painter Inlier (Heathgate Resources, 1998). The increase in the dominance of chloride seems to follow the lateral positions of each water group, with Black Spring and PHS plotting between the Mt. Painter Inlier waters to the west and the Willawortina Formation to the east. Chemical data on local bore water from GAB aquifers are limited. Generally, in the southwestern part of the GAB where the MPD and Lake Frome plains are located, groundwater is characterised by Na–Cl–SO_4 type (Habermehl, 1998a). In contrast, the PHS water is characterised by a Na–Cl–HCO_3 type water.

5.3. Trace elements

The trace element concentrations in the PHS change into different ways downstream (Table 2; Fig. 7) that can be grouped in trends:

(A) Al, Cu, Pb, Y, Zn and REE concentrations drop by a factor of 4 or more from Pool 1 to Pool 2, and then remain constant downstream (e.g., Zn and Y in Fig. 7a,b). Although minerals (e.g., rutile) may have sorbed the trace elements, this

Table 2
Trace element and stable isotope analyses of waters from the Paralana Hot Springs and Mt. Painter Inlier

Element	Units[1]	Pool 1			Pool 2	PC 1	PC 2	Black Spring	Boulder Bore	No. 6 Workings Well	Radium Creek Bore	Arkaroola Spring
		This study	Grant (1938)[2]	Heathgate (1998)[2]								
Ag	ppb	0.029	1[2]		0.024	0.019	0.020	0.033	0.029	0.028	0.021	0.017
Al	ppb	5.41	100[2]	<50[2]	1.29	0.66	0.47	5.71	1.20	2.95	2.25	1.61
As	ppb	37.4		<100[2]	38.3	38.5	40.3	45.8	18.5	68.4	19.5	22.0
Au	ppb	0.361			0.321	0.312	0.312	0.408	0.308	0.376	0.312	0.309
B	ppm	0.19	0.8	0.21	0.19	0.19	0.20	0.39	0.3	0.18	0.10	0.17
Ba	ppb	93.8	200[2]	100[2]	92.6	89.7	89.5	22.8	28.1	19.0	64.3	104
Cd	ppb	0.138		<10	0.112	0.116	0.123	0.039	0.060	0.111	0.292	0.050
Co	ppb	0.247	<3	<20	0.206	0.212	0.224	1.231	0.373	1.79	0.839	0.751
Cr	ppb	2.75	2	<30	2.45	2.52	2.55	4.65	4.79	9.43	3.24	2.84
Cs	ppb	16.2	400		16.4	17.0	17.5	0.456	0.003	0.106	0.288	<0.003
Cu	ppb	10.9	12	<20	5.26	5.11	5.14	13.6	8.54	31.4	5.41	4.95
Fe	ppm	0.06	0.02	0.69	0.06	0.03	0.02	0.41	<0.01	0.08	<0.01	<0.01
Ga	ppb	2.94			2.88	2.73	2.68	6.60	0.77	4.99	1.87	2.99
Ge	ppb	3.10	2		2.98	3.23	3.08	0.713	0.761	1.61	0.567	0.357
Li	ppm	0.049	0.6		0.051	0.051	0.049	0.125	0.024	0.030	0.029	0.004
Mn	ppb	97.3	1	<20	82.1	29.7	8.74	392	1.15	718	24.6	33.0
Mo	ppb	32.8	60	<50	33.0	33.8	36.1	2.80	8.01	23.3	57.5	2.07
Nb	ppb	0.045			0.009	<0.001	<0.001	0.303	<0.001	0.157	0.006	<0.001
Ni	ppb	6.68	<3	50	5.16	5.20	5.38	12.0	8.65	31.0	16.3	8.35
Os	ppb	0.351			0.230	0.272	0.334	0.800	0.486	0.758	0.215	0.188
Pb	ppb	0.495	5		0.132	0.113	0.089	0.422	5.40	0.147	0.527	0.307
Pd	ppb	0.357			0.336	0.360	0.378	1.166	0.788	2.55	1.180	0.880
Pt	ppb	0.00054			0.005	0.004	0.005	0.006	0.005	0.006	0.005	0.005
Rb	ppb	195			196	201	205	151	19.0	4.61	13.5	5.94
Re	ppb	0.0041			0.004	0.004	0.004	0.012	0.016	0.270	0.291	0.007
Rh	ppb	0.0348			0.033	0.036	0.037	0.087	0.066	0.214	0.085	0.066
S	ppm	47			48	48	48	28	75	59	43	21
Sb	ppb	0.608			0.510	0.503	0.509	0.123	0.005	0.086	0.042	0.139
Sc	ppb	17.1			16.7	17.4	18.2	23.5	6.31	26.1	12.0	4.85
Se	ppm	0.01		<0.01	0.01	0.02	0.02	0.02	0.02	0.04	0.03	0.02
Si	ppm	34.3			34.5	34.5	34.7	32.5	8.7	35.5	16	6.1
Sn	ppb	0.058	10		0.0014	<0.005	<0.005	0.164	0.009	0.221	0.066	0.062
Sr	ppb	339	500		341	347	351	600	530	1299	634	496
T1	ppb	0.574			0.454	0.496	0.500	0.0351	0.0083	0.0217	0.0101	0.0071
U	ppb	0.0704		250	0.169	0.304	0.295	2.90	5.71	318	665	1.58
V	ppb	17.8	3	<50	19.6	20.7	21.7	36.6	16.2	37.4	13.5	11.9
W	ppb	11.0	3		11.3	10.2	10.7	1.08	<0.01	0.027	0.057	<0.01
Y	ppb	0.395			0.0121	0.009	0.005	0.954	0.025	0.095	0.596	0.047
Zn	ppb	11.4	<30	<20	2.13	1.65	1.29	15.9	4.49	2.01	6.89	7.81
La	ppb	0.0149			0.0102	0.0055	0.0033	0.864	0.0143	0.0261	0.0249	0.0051
Ce	ppb	0.0410			0.0377	0.0256	0.0152	1.43	0.0644	0.0741	0.0315	0.0091
Pr	ppb	<d.l.			<0.001	<0.001	<0.001	0.172	<0.001	0.003	0.002	<0.001
Nd	ppb	0.0039			0.0023	<0.001	<0.001	0.730	0.0069	0.0255	0.0218	0.0016
Sm	ppb	0.0010			0.0005	<0.001	<0.001	0.158	<0.002	0.0075	0.0075	0.0012
Gd	ppb	<d.l.			<0.001	<0.001	<0.001	0.246	<0.002	0.0087	0.0153	<0.001
Tb	ppb	<d.l.			<0.001	<0.001	<0.001	0.0283	<0.001	<0.001	<0.001	<0.001
Dy	ppb	<d.l.			<0.001	<0.001	<0.001	0.161	<0.001	0.0065	0.0315	<0.001
Ho	ppb	<d.l.			<0.001	<0.001	<0.001	0.0261	<0.001	0.0032	0.0075	<0.001
Er	ppb	<d.l.			<0.001	<0.001	<0.001	0.0777	<0.001	0.0055	0.0332	<0.001

Table 2 (*continued*)

Element	Units[1]		Pool 1	Pool 2	PC 1	PC 2	Black Spring	Boulder Bore	No. 6 Workings Well	Radium Creek Bore	Arkaroola Spring
Tm	ppb	<d.l.		<0.001	<0.001	<0.001	0.0078	<0.001	<0.001	0.0035	<0.001
Yb	ppb	<d.l.		<0.001	<0.001	<0.001	0.0482	<0.001	<0.002	0.0252	<0.001
$\delta^{18}O$	‰	−6.4				−6.3	−4.7	−6.6	−5.0	−6.7	
$\delta^{2}H$	‰	−45				−44	−33	−47	−40	−44	
$\delta^{13}C$	‰	−11.1				−12.1	−9.9	−8.7	−9.6	−11.5	

[1] Elements quoted in ppm were measured by ICP-AES and those in ppb by ICP-MS; [2] All concentrations from Grant (1938) and Heathgate Resources (1998) were quoted in ppm and are converted to ppb as required. Europium concentrations are not reported because of analytical mass interface (ICP-MS) from barium oxide. δ^{18} O and δ^{2} H are referenced to VSMOW and δ^{13} C is referenced to VPDB (e.g., Clark and Fritz, 1997).

is unlikely because the water would not have reacted with the minerals over such a short distance (2–3 m), i.e., a small surface area of rock relative to cubic metres of water, plus the bottom of Pool 2 was covered in organic matter and biota. The most likely explanation is increased sorption onto the organic matter, or uptake by the abundant cyanobacteria and other organisms in Pool 2, especially for micronutrients such as Cu and Zn;

(B) Mn and Fe concentrations are constant or drop slightly between Pool 1 and Pool 2 and then decrease by a factor of 2 to 10 in Hot Springs Creek (e.g., Fe in Fig. 7c) and is probably because of uptake by organisms and perhaps precipitation of Mn and Fe oxyhydroxide minerals on cooling, although no staining was observed in Hot Springs Creek;

(C) U concentration increases from Pool 1 to PC1 (0.07 to 0.30 pbb; Fig. 7d), probably because U becomes more soluble under oxidising conditions and leaches out of uriniferous rocks and sediments outcropping around the springs (e.g., Coats and Blissett, 1971; Neumann et al., 2000); and

(D) Li, W, Mo and Rb concentrations remain constant from Pool 1 to PC2 (Fig. 7e,f).

In comparison to other groundwaters in the Mt. Painter Inlier, the PHS have high concentrations of Rb, Mo, and W (Table 2). Lithium concentrations are comparatively high in PHS and Black Spring. As the only source of Li is from minerals such as tourmaline, biotite and other micas, Li concentrations are an indication of the extent of water/rock interaction. Both springs also have similar Cl/Br ratios. The similarity of the chemistry of PHS and their relative positions along the Paralana fault system and Black Spring suggest that Black Spring and PHS have the same water source along the Paralana fault zone.

Table 3
Composition of gas from Pool 1 compared to atmospheric composition (in vol.%)

		Ratio		Dry gas concentration				
		$\%O_2/\%N_2$	$\%CH_4$	$CO_2\%$	$\%O_2$	$\%N_2$	%CO (ppm)	%He
April	1	0.182	0.014	5.200	14.57	80.2	<2	0.0846
	4	0.202	0.010	3.810	16.15	80.0	<2	0.0620
July	1	0.219	0.011	3.910	17.26	78.8	<2	0.0390
	2	0.199	0.011	4.500	15.87	79.6	<2	0.0400
	3	0.205	0.008	3.820	16.37	79.8	<2	0.0350
	4	0.202	0.009	3.990	16.11	79.9	<2	0.0380
	5	0.199	0.010	4.200	15.89	79.9	<2	0.0360
Average		0.201	0.010	4.204	16.03	79.7	<2	0.0478
Atmosphere		0.268	0.00017	0.036	20.95	78.08	<2	0.0005
Grant, 1938				11.9		88.1		0.056

Atmosphere composition from Oxtoby and Nachtrieb (1996).

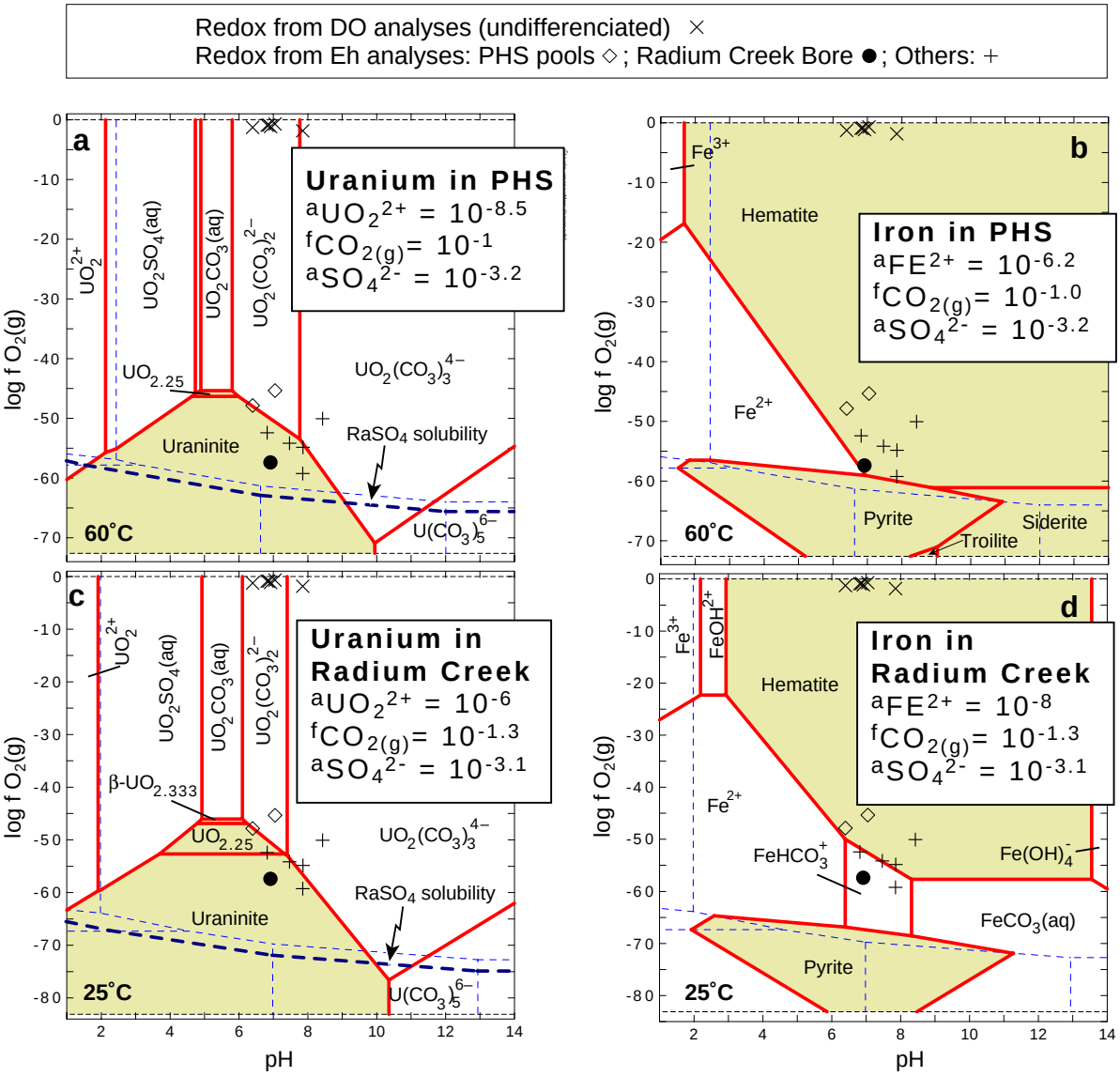

Fig. 5. Log fO_2(g) vs. pH diagrams illustrating U and Fe speciation in the PHS fluid (a, b) and in the Radium Creek Bore fluid (c,d). The field pH and redox of regional waters are plotted; the redox states obtained from the DO and Eh measurements are both reported. The thick dashed lines in (a,c) indicate the solubility of $RaSO_4$(s) in equilibrium with $aRa^{2+} = 85.4\ 10^{-6}$ (approximatively 14 Bq/L Ra), and the thin dashed lines in all diagrams show the sulphur sub-diagram.

The LREE (light Rare Earth Elements) content of the PHS is similar to that of the other analysed waters of the region, with the exception of Black Spring, which contains in excess of one order of magnitude more LREE (Table 2; Fig. 8). HREE (heavy Rare Earth Elements) were measured reliably only in Black Spring and Radium Creek Bore. The high REE contents of Black Spring are attributed to concentration by the abundant biomass in this spring. Radium Creek Bore is characterised by an enrichment of HREE relative to chondrite; this is unusual for granite-hosted waters (e.g., van Middlesworth and Wood, 1998), and may be related to unusual mineralogical composition of the hosting, Th, U and

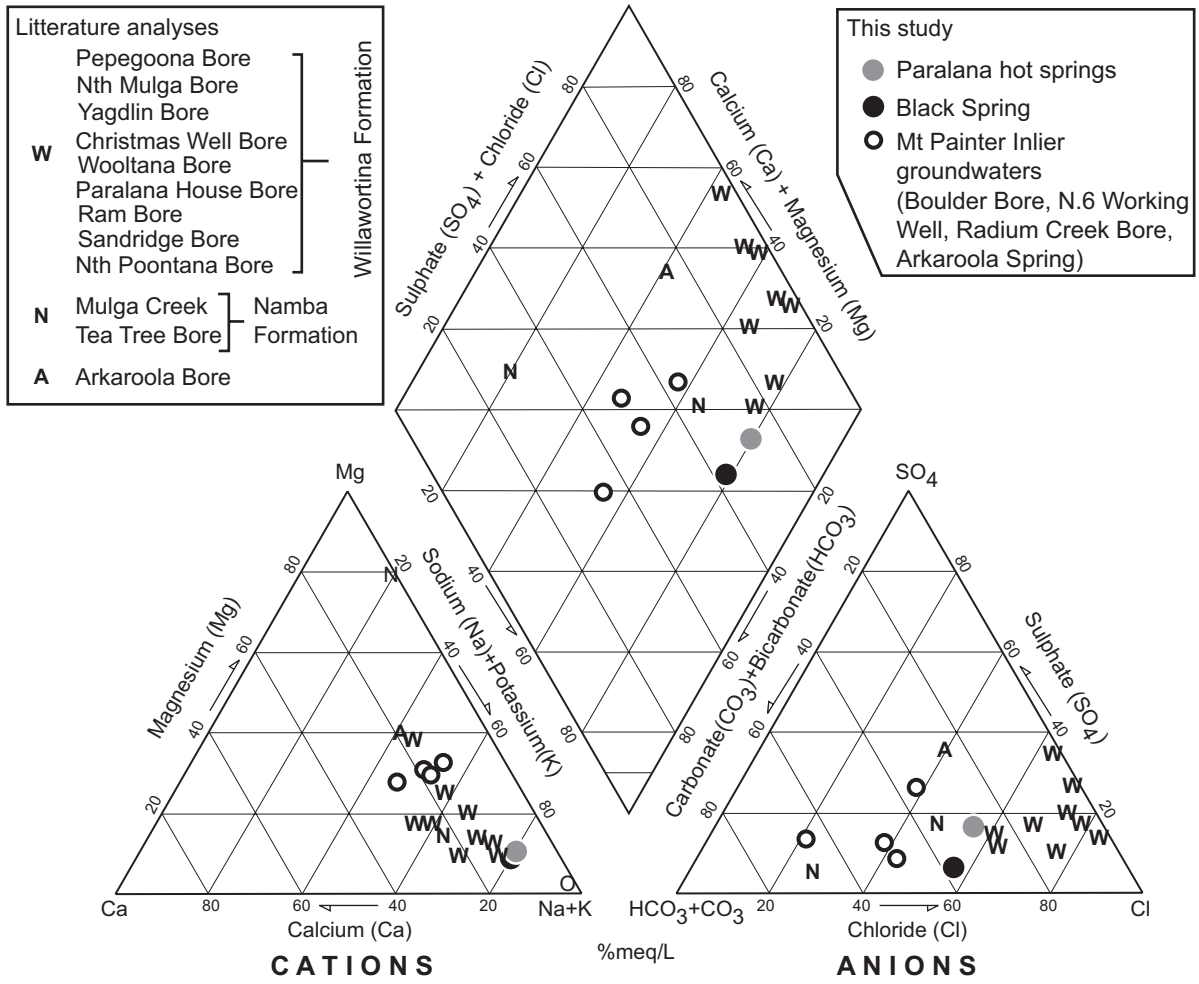

Fig. 6. Piper diagram comparing the major elemental chemistry of sampled waters from the Mount Painter Domain with that from water from the Frome Embayment plains (regional waters from Heathgate Resources, 1998).

REE-rich Proterozoic granite (Sandiford et al., 1998a).

PHS have the lowest U concentration among sampled waters (Fig. 7d; <0.1 ppb), lower than the 0.5 to 10 ppb range reported by Dahlkamp (1993) as characteristic for groundwaters world-wide. These values plot near the solubility line of uraninite for the Eh-pH conditions of pool 1 (Fig. 5a). PHS also contain elevated Ra concentrations of 24.5 Bq/L (Pool 1; Heathgate Resources, 1998), corresponding to 0.38 ppb Ra; Black Spring has 0.06 Bq/L, a value representative of the other surface waters of the region (Heathgate Resources, 1998). The Ra concentration in PHS indicates that these waters are highly supersaturated with respect to $RaSO_4$(s) (Fig. 5a,c). This may indicate lower sulphate concentrations at depth, either as a result of more reducing conditions, or mixing with sulphate-bearing waters on the way up to the springs. No. 6 Working Well and RC clearly stand out as the only groundwater carrying high concentrations of uranium. These concentrations can be related to the U-rich Proterozoic granites and gneisses in which these two springs are located (see below). Speciation calculations indicate that U tranport in these waters is mainly as uranyl carbonate complexes (e.g., $UO_2(CO_3)_2^{2-}$). Considering that mineralising aquifers commonly contain 10–400 ppb U (Dahlkamp, 1993), No.6 Workings

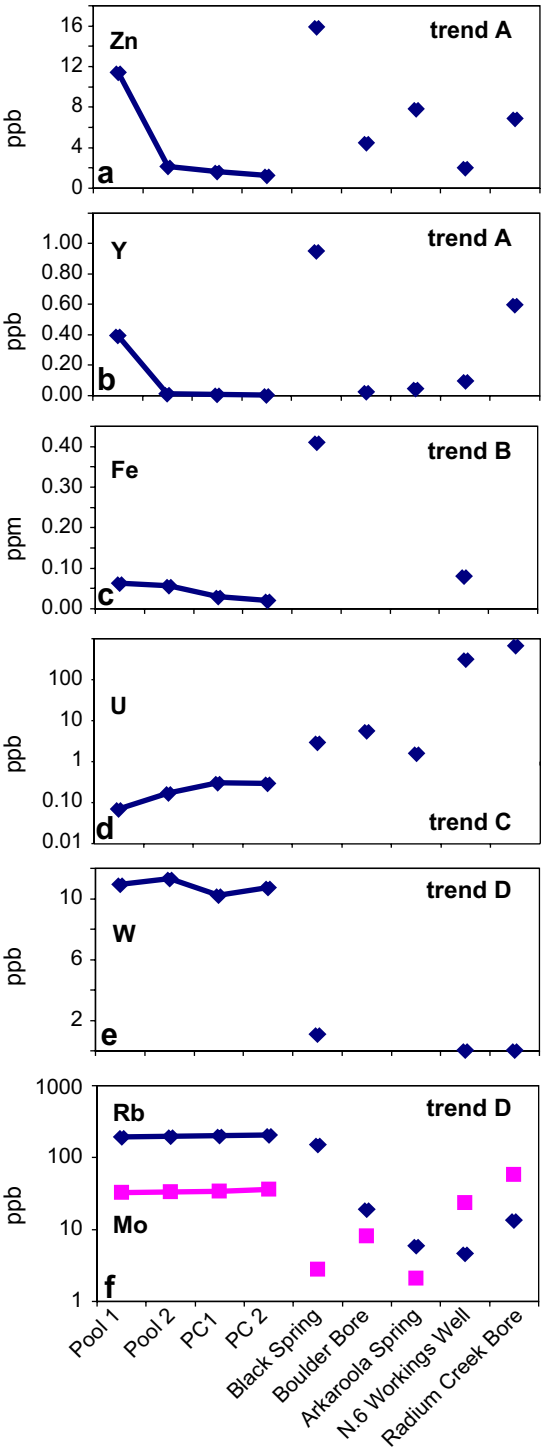

Fig. 7. Comparison of concentrations of some trace elements among the Mt. Painter Domain waters. Data in ppm.

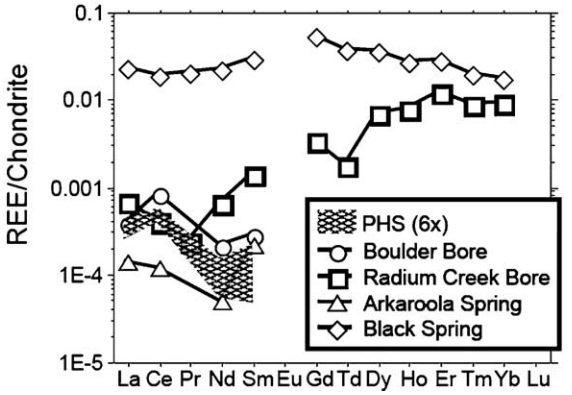

Fig. 8. REE patterns of waters from the Mt. Painter Domain. Chondrite data from Evensen et al. (1978).

Well and, in particular, RC are potential sources for U-mineralisation.

5.4. Mineral saturation states

Mineral saturation states (Table 4) were determined for all sampled waters using Geochemist's Workbench (GWB) V 4.0.3 (Bethke, 1998) and the thermodynamic properties in the database distributed by the Lawrence Livermore National Laboratory (Version 8, Revision 6). Minerals with saturation indices (SI) between −1 and 1 are likely to control the concentration of elements in the water. Minerals with SI much larger than 1 are strongly over saturated; this may be linked to kinetic problems (e.g., $Fe(OH)_3$(am) precipitating instead of hematite), to poor thermodynamic properties for the mineral or aqueous species, or to particulate matter reaching through the filter.

The composition of the Pool 1 water appears to be controlled by clay minerals (e.g., celadonite, smectite), zeolite (laumontite), and by common rock-forming minerals such as albite and epidote (assuming reducing condition). SiO_2(aq) is next to equilibrium with chalcedony. The Ba content is close to equilibrium with witherite and barite. Pool 1 is only slightly undersaturated with respect to uraninite and coffinite for redox conditions corresponding to the Eh measurement. Hence it appears that the mineral assemblage inferred to control the chemistry of PHS water is consistent with the observed regional rocks and alteration, as well as with the fossil Mt. Painter–Mt. Gee epithermal system.

Table 4
Saturations indices for waters from the Mt. Painter Complex

	Ag	Au	Cu	Pd	Albite	Barite	Beidellite-K	Beidellite-Na	Boehmite	Calcite	Celadonite	Cerussite	Chalcedony	Coffinite
Pool1 (Eh)	0.9	16.4	−1.1	8.8	0.6	0.1	3.2	3.3	0.9	−0.9	1.3	−2.2	0.3	−1.8
Pool2 (Eh)	0.6	16.7	−1.8	7.0	0.6	0.2	1.8	2.0	0.1	−0.2	2.5	−1.3	0.5	–
PC2 (Eh)	1.9	18.4	−0.6	10.2	0.6	0.2	2.1	2.2	0.0	−0.6	2.0	−2.3	0.6	−0.3
Radium Creek Bore (Eh)	–	20.3	0.0	12.2	1.2	0.2	4.4	4.7	1.2	0.0	2.6	−0.9	0.5	2.9
No. 6 Working Well (Eh)	3.4	21.9	1.4	13.6	3.8	0.8	5.5	5.8	0.6	1.6	7.8	−0.2	1.1	1.4
Black Spring (Eh)	3.0	20.7	0.5	11.0	2.0	0.5	3.8	3.9	0.8	0.9	5.0	0.0	0.5	−2.6
Arkaroola Spring (Eh)	2.8	19.8	0.1	8.7	−0.6	0.1	−0.8	−0.5	1.2	3.9	0.3	0.0	–	3.9
Boulder Bore (Eh)	2.8	19.9	0.1	10.6	0.1	0.0	1.8	1.8	0.4	0.2	2.9	0.5	0.2	−0.8

	Dolomite (ord)	Epidote	Fluorite	Goethite	Gypsum	Hematite	Heulandite	Illite	Jadeite	Kaolinite	K-Feldspar	Laumontite	Magnesite	Magnetite
Pool1 (Eh)	−0.7	−2.0	−0.7	1.2	−1.8	3.5	2.4	3.2	−1.7	3.2	1.8	0.8	−1.3	1.2
Pool2 (Eh)	0.6	3.3	−1.9	7.7	2.5	2.3	−1.8	1.8	2.0	0.4	−0.7	6.3	2.6	1.3
PC2 (Eh)	−0.2	–	−0.6	0.8	−1.9	2.6	2.5	2.3	−1.9	2.0	2.0	0.1	−1.1	−0.1
Radium Creek Bore (Eh)	1.2	–	−0.4	–	−1.6	–	4.4	4.6	−1.2	4.3	2.6	2.0	−0.5	–
No. 6 Working Well (Eh)	4.7	–	−1.1	–	−1.2	–	9.2	6.5	0.8	4.3	5.0	5.0	1.4	–
Black Spring (Eh)	2.6	–	–	–	−1.9	–	5.5	4.7	−0.4	3.4	3.6	2.8	0.1	–
Arkaroola Spring (Eh)	–	−2.8	–	−2.2	–	0.4	0.8	−2.5	−0.1	1.3	−0.5	1.0	–	1.1
Boulder Bore (Eh)	1.9	–	−1.7	–	−1.7	–	1.7	2.6	−2.0	2.1	2.0	0.0	0.1	–

	Montmor-K	Mordenite	Natrolite	Paragonite	Quartz	Rhodochrosite	Saponite-Mg	Scolecite	Smectite (low-Fe)	Smithsonite	Strontianite	Talc	Uraninite	Witherite
Pool1 (Eh)	3.0	1.0	−1.9	2.7	0.6	−1.7	−1.7	1.7	0.8	−2.5	−1.4	−2.3	−1.6	0.1
Pool2 (Eh)	−2.2	1.0	0.7	−1.1	1.3	1.3	1.8	−2.7	−0.7	0.9	–	1.0		
PC2 (Eh)	2.7	1.5	−2.6	1.0	0.8	−2.4	−0.7	0.9	0.6	−3.0	−1.0	−0.9	−0.4	0.7
Radium Creek Bore (Eh)	4.4	2.2	−1.0	4.0	0.8	−1.7	−0.6	3.0	–	−2.0	−0.3	−1.2	2.9	1.2
No. 6 Working Well (Eh)	6.7	5.4	2.6	5.4	1.3	1.2	8.3	5.5	–	−1.3	1.4	7.7	0.9	3.1
Black Spring (Eh)	4.5	2.6	0.6	3.9	0.8	0.6	3.6	3.8	–	−0.8	0.7	2.9	−2.6	2.8
Arkaroola Spring (Eh)	−0.7	−3.0	−1.2	0.3	0.0	7.0	0.9	–	−1.1	1.0	6.3	–	2.8	
Boulder Bore (Eh)	2.6	0.4	−2.3	1.3	0.5	−2.6	1.9	1.3	–	−1.9	0.0	1.3	−0.5	1.2

Mineral saturation states do not change significantly from Pool 1 to PC 2 despite the decrease in temperature and the change in redox conditions. Gold is supersaturated in all waters analysed apart from Arkaroola Spring where the gold analysis was not included in mineral saturation calculations.

5.5. Stable isotopes: hydrogen, oxygen and carbon

Isotopic ratios for all sampled waters range between −6.7 to −4.7 δ^{18}O VSMOW and −33 to −47 δ^{2}H VSMOW (Table 2; Fig. 9). These values are plotted against the Local Meteoric Water Line (LMWL) using data from Alice Springs, about 800 km North and located in a similar arid environment (AEA/WMO, 2004). All waters are close to the LMWL, with the exception of No. 6 Working Well. The ^{18}O and ^{2}H isotopic composition of No. 6 Workings Well can be explained by a few percent of evaporation of a Radium Creek Bore type water (Fig. 9). Stable isotopes suggest that the difference between Black Spring and PHS is related to different fluid pathways and/or climatic control.

Oxygen and hydrogen isotopic ratios in the PHS do not show evidence of hot water/rock interaction, which result in waters plotting to the right of the LMWL. This suggests that either the water had a short residence time and little chance to interact with the local geology, or that the waters have not reached high enough temperatures to initiate significant water/rock interaction, or that the system was fluid buffered. Large-scale mixing with meteoric waters is also a possibility, which would dilute the effects of water/rock interaction.

Isotopic ratios for dissolved inorganic carbon (δ^{13}C) in all sampled waters lie in the range −12.3‰ to −8.7‰ VPDB (Table 2), indicating a biological origin (C_4-type plants). δ^{13}C values for the gas sampled from Pool 1 range from −18.1‰ to −19.0‰ VPDB, much lighter than δ^{13}C from magmatic (mantle) CO_2 (−3.5 ± 0.5; e.g., Hoefs, 1997), and also characteristic for a biological origin. The small δ^{13}C fractionation of 7‰ to 8‰ between CO_2(g) and dissolved carbonate indicates that both water and gas are in equilibrium with respect to carbon. Assuming that most of the dissolved carbon resides as HCO_3^- and using the constants provided by Deines et al. (1974) for carbon isotope equilibrium between $HCO_{3(aq)}^-$ and $CO_{2(g)}$, the isotopic composition of the bicarbonate in equilibrium with the Paralana Hot Spring CO_2(g) (δ^{13}C = −18.1 to −19) is calculated to be between −12.6 and −13.5 at 57 °C, and −10.4 and −11.3 at 25 °C.

5.6. Gas analysis

The gas emanating from Pool 1 in PHS has elevated concentrations of CO_2(g), CH_4(g), He(g) and a diminished concentration of O_2(g) compared to the atmosphere (Table 3). The isotopic composition of

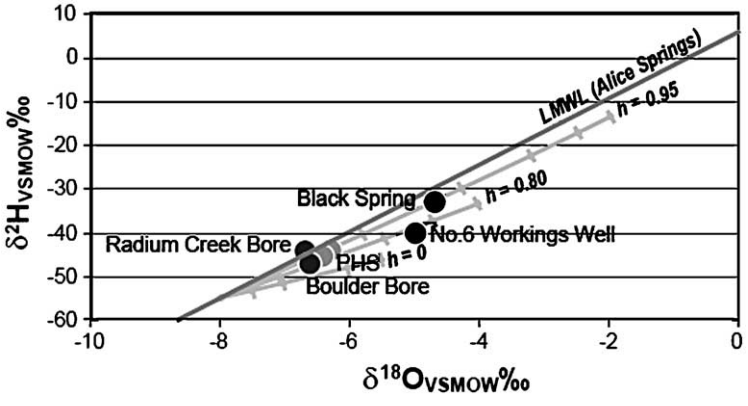

Fig. 9. Stable isotopic composition of water from the Mt. Painter Inlier, compared to the Local Meteoric Water Line (LMWL) from the Alice Springs precipitation data (AEA/WMO, 2004). The greyed lines show the stable isotope composition of an evaporating water body with composition on the LMWL, calculated following Gonfiantini (1986) for relative humidity (h) of 95%, 80% and 0%. The curves are drawn for remaining fractions values between 100% and 90%, with ticks at 2% interval. The isotopic composition of the atmospheric water is assumed δ^{2}H = −86 and δ^{18}O = −12, temperature = 25 °C, equilibrium fractionation factors from Kakiuchi and Matsuo (1979).

carbon shows that CO_2(g) is sourced from soil, plants or fresh-water carbonates. CO_2(g) therefore most likely results from the oxidation of biological carbon in the soil or at the bottom of the pool. The Rn levels around PHS are extremely high (Fig. 10); such concentrations are normally reported only from cave systems, were Rn is concentrated by gravity and can travel fast in air and water to the traps. A significant proportion of the He may be produced by alpha decay of U, Th and their decay products. The Rn contents of PHS indicate relatively fast water uplift and the presence of rocks enriched in U at shallow depth on the flow path of the PHS fluid.

5.7. Petrography of hydrothermally altered rocks at the Paralana hot springs

Rock samples collected from the outcrop adjacent to Pool 1 (Fig. 4b) have been strongly affected by hydrothermal fluids, showing evidence of early mesothermal mineralisation followed by multiple stages of epithermal overprint. Mesothermal quartz veins are associated to minor amounts of epidote and consist of granuloblastic, undulose quartz crystals with serrated grain boundaries and fluid inclusions. These veins have been fractured and brecciated, with early quartz crystals showing evidence of adiabatic shock through needle-like slivers being sheared off their edges. Fractures have been infilled with chalcedony and recrystallised quartz, which has eroded the early quartz and healed the adiabatic shock textures. The resultant breccia is matrix supported with angular to rounded clasts and contains coarser grained opaques. Early carbonate clasts are either replaced by chalcedonic silica and rimmed with opaques, or form cavities which are subsequently lined with the most recent mineralisation. Repeated fracturing and infilling has produced at least three identifiable generations of epithermal chalcedonic silica.

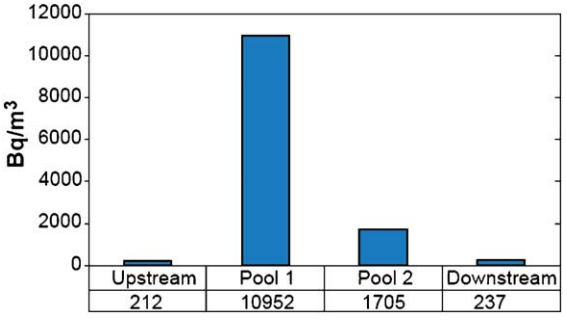

Fig. 10. Radon concentrations around the Paralana Hot Springs.

Muscovite is introduced in the second generation. Iron mineralisation records the changing redox conditions of the mineralising fluid; pyrite present in the early mesothermal veins and rimming carbonate clasts indicates reducing conditions and later hematite, found in cross-cutting recrystallised quartz veins and lining cavities, indicates more oxidising conditions. As pyrite is fresh, it is assumed that redox conditions remained near the hematite–pyrite boundary (Fig. 5). Cavities contain opaline silica, gypsum, hematite, kaolinite (this study) and rare torbernite (Coats and Blissett, 1971), which represent the most recent mineralisation. Note that the gypsum is not associated with pyrite, and is interpreted to represent direct precipitation from the hydrothermal water and is not a weathering product.

Textures found in rocks at Pool 1 were controlled by movements along the Paralana fault, which have resulted in a long history of overprinting structures, textures and mineralisation. The evidence seen on a small scale, coupled with the numerous dilational jogs along the fault zone suggests that the Paralana fault is a long lived fluid conduit in which fluids have been boiling (adiabatic textures), high temperature (muscovite) and low temperature (opaline silica, gypsum). The late opaline silica and gypsum indicate that the system has most recently been at low temperature.

6. Discussion

6.1. Paralana Hot Springs: fluid flow and heat sources

6.1.1. Geothermometry

Geothermometry is used to determine the temperature at which a hydrothermal water last reached equilibrium with respect to particular host rock minerals, assuming that little equilibration occurred during the transport to the surface, that nothing was lost to the vapor phase, and that no mixing between thermal and surface waters occurred. Studies on active geothermal systems show that the content of SiO_2 (solubility of quartz and other SiO_2 forms) and Na–K–Ca (as con-

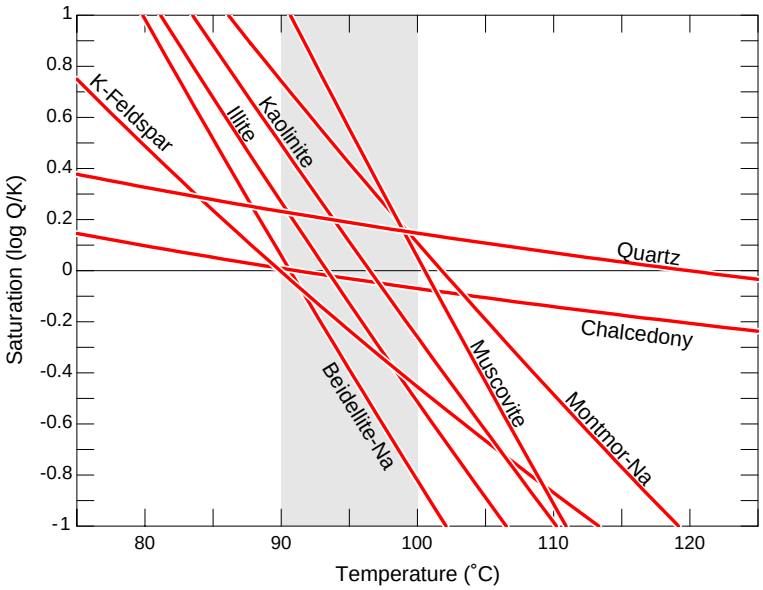

Fig. 11. Saturation indices of selected minerals as a function of temperature for the Pool 1 sample.

trolled by feldspars, clay minerals and micas) can lead accurate geothermometric data under favorable circumstances (e.g., Mazor et al., 1980). Mineral saturation indices were calculated as a function of temperature using GWB. All the calculations were performed using the Eh values, but the geothermometric calculations are mainly redox independent. Mazor et al. (1980) and Arnorsson (1975) showed that at $T<\sim110$ °C, chalcedony controls SiO_2 concentrations in thermal waters, whereas above ~180 °C quartz is the controlling phase. For PHS, chalcedony is saturated at 92 °C, whereas quartz is saturated at 120 °C (Fig. 11). The relatively low temperature of equilibration and the observation of chalcedony overprinting quartz in the hydrothermally weathered outcrop next to Pool 1 suggest that 92 °C is the best estimate for the temperature of last equilibration. The calculations of the equilibrium state of alumino-silicates show that common rock-forming minerals such as K-feldspar and muscovite, as well as common weathering minerals of granitic rocks such as illite, montmorillonite and beidellite all equilibrate between 90 and 100 °C (Fig. 11). Hence, the most likely last temperature of equilibration for water–rock interaction of the PHS water is 95 ± 5 °C.

6.1.2. Heat sources and geothermal gradient

A minimum heating of 65 °C is required to bring a meteoric water (~25 °C) to the temperature of last equilibration of the PHS (≥90 °C). Radiogenic heating of PHS water is supported by the high Rn and He contents and by the occurrence of several rock types in the MPD containing elevated concentrations of heat-generating elements (Table 5). Over a year,

Table 5
Average heat generation in selected Mt. Painter Province lithologies

Lithology	U [ppm]	Th [ppm]	K [ppm]	U [μ W/kg]	Th [μ W/kg]	K [μ W/kg]	Total [μ W/kg]	Mass[1] of rock required [t/year]
British empire granite[2]	16	11	49,000	0.00155	0.00029	0.00017	0.00201	4290
Hot springs gneiss[3]	75	288	41,700	0.00725	0.00757	0.00015	0.01497	576
Freeling heights quartzite[2]	1.8	7.1	20,000	0.00017	0.00019	0.00007	0.00043	20,100
Paralana gneiss[2]	103	264	33,000	0.00996	0.00694	0.00012	0.01702	507

[1] Mass of rock required to raise the temperature of 1 kg water by 65 °C over a year, assuming heat capacity values for pure water. [2] Concentrations data from Sandiford et al. (1998a). [3] Concentrations data from Neumann et al. (2000).

the energy necessary for heating 1 kg of water by 65 °C is generated by as little as 507 t of Paralana Gneiss (Table 5). For a less enriched granite such as the British Empire Granite, 4300 t of rock are required.

Estimates of the geothermal gradient in the two possible source areas (MPD and GAB) can be used to constrain the depth of circulation required to produce the 90–100 °C temperature of last equilibration between rock and fluid as indicated by the geothermometric analysis. The surface heat flow (Q, W/m^2) is related to the geothermal gradient (B, °C/m) and the thermal conductivity of the host rock (λ, W/m/K) by the expression:

$Q = \lambda B$ (Cull, 1991).

In the MPD, a heat flow measurement of 126 mW/m^2 is available from the Parabana Hill, 34 km NE of the PHS (Cull, 1982). The hill consists of Terrapina Granite, thus the thermal conductivity of granite, ranging from 2800 to 4600 mW/m/K (Roy et al., 1981), can be used to constrain the local geothermal gradient in the range 27 to 45 °C/km. This indicates that the temperature of 90–100 °C was achieved between 1.4 and 2.4 km.

Estimates from the geothermal gradient in the GAB range from 15.4 to 102.6 °C/km, with a mean of 48 °C/km (Polak and Horsfall, 1979), which compares with a world average of 33 °C/km for continental sedimentary basins (Lee and Uyedas, 1965). The highest values (>70 °C/km) are found in the Northern (Fort Bowen Ridge) and Southern (Bulloo Embayment, 300 km East of the Lake Frome Embayment) parts of the basin, and have been related to radioactive Proterozoic basement (Howard and Sass, 1964). Temperatures of water in wells tapping GAB typically range from 30 to 50 °C; however, the top aquifer in the GAB is located at depths in excess of 2000 m in the central part of the basin (Cox and Barron, 1998), so temperature in many sub-basins of the GAB reach up to 100 °C at the well head (Cull and Conley, 1983). At the Berverley mine (Fig. 1b), the top of the GAB is represented by the Cadna-Owie Formation at ~300 m below the surface; the water in this aquifer is at 50 °C (Heathgate Resources, 1998). Temperatures of GAB spring waters are lower, reaching 40 °C (Habermehl, 1998a), and it is unlikely that a spring formed by the same mechanism as a GAB mound spring could reach temperature of 57 °C, given the shallow aquifer source for these springs.

6.1.3. Fluid flow

The close proximity of the PHS and Black Spring to the Paralana fault system suggests that the fault provides a conduit for groundwater. The detailed geometry of the PHS fault is poorly known, and the fault could tap waters from either MPD or the GAB. The potential to provide access to heat sources and flow paths which could produce a temperature of 60 °C and flow rate of 16 L/s must be evaluated for both the GAB and MPD to consider both as prospective fluid sources for the PHS.

6.1.4. GAB source

Groundwater movement in the GAB is slow, with a probable flow rate between 1 and 5 m/year, due to low hydraulic conductivities and hydraulic gradients and high porosities in the aquifers (Habermehl, 1998b). This results in long residence times, which have been determined from ^{14}C and ^{36}Cl studies to range from several thousands of years in recharge areas to 1.4 million years at the centre of the basin (Habermehl, 1998b). If PHS is sourced from a GAB aquifer, we would expect it to have a residence time in excess of 1 million years (~1000 km from the recharge area in the Springsure area, Queensland (Cox and Barron, 1998). The range of flow rates from mound springs (1–150 L/s) sourced from the GAB demonstrates that even with the slow groundwater movement throughout the basin, a fracture or fault mechanism producing a conduit for groundwaters can produce flow rates of 16 L/s. The lack of a mound structure at the PHS, or any evidence of travertine, calcrete, calcareous or carbonaceous precipitation suggests that the waters are not from the same GAB mound spring system. It is improbable that fluids from the Cadna-Owie Formation flow directly upwards to the PHS as the hydraulic head (90 m) is too low to reach the springs. This flow path may be possible if the aquifer is tapped by a structural feature connected to the Paralana fault system, however, the water would require deeper circulation to elevate the pressure head and drive the fluid up a conduit to the springs.

6.1.5. Mount Painter domain source

Many maps of the MPD incorporating the PHS show the Freeling Heights plateau draining into Hot Springs Creek and eventually into PHS (Coats and Blissett, 1971; GSSA, 1983; Sprigg, 1984). Black Spring, which is found at a similar elevation to PHS along the Paralana fault, may derive its fluids from the MPD in a similar fashion.

Surface infiltration from precipitation in the MPD would rely primarily on gravity-driven flow through hydraulic gradients and fracture systems to circulate through the rocks. A W–E schematic geological cross-section of the MPD (Fig. 3) shows that water from either Mt. Painter or Freeling Heights would flow through gneisses, schists and granites of the MPD to reach the Paralana fault and as a result, PHS. A rough estimate of the residence time for this scenario can be calculated on the basis of Darcy's law ($V = -\frac{K}{n}\frac{dh}{dl}$; V is the average linear velocity at which water is moving, K the hydraulic conductivity, n the porosity, and dh/dl the hydraulic head gradient). Assuming that the flow is directly from the Freeling Heights to the springs, $dh/dl = 700\ m/10\ km = 0.07$. The basement rocks have low primary porosity and hydraulic conductivity. Unfractured igneous and metamorphic rocks typically have hydraulic conductivities ranging between 10^{-13} and 10^{-10} m/s and primary porosities ranging from 0% to 5% (Domenico and Schwartz, 1998; Freeze and Cherry, 1979). On average the porosity of crystalline rocks can be increased by 2–5% by fracturing, while weathering can produce porosities of 30–60% in plutonic and metamorphic rocks (Fetter, 1994). While both physical and chemical weathering do occur in the MPD, it is unlikely that porosities of this magnitude exist within the domain. Thus, a porosity range between 2% and 5% is assumed. Hydraulic conductivities are also increased in fractured igneous and metamorphic units to a range of 10^{-9} to 10^{-5} m/s (Domenico and Schwartz, 1998; Freeze and Cherry, 1979). Using the above assumption, the calculated average velocity range from 1.4×10^{-5} to 1.4×10^{-9} m/s, implying that it would take from 9 to 226,500 years for surface infiltration at Mt. Painter to flow the 10 km directly to PHS.

One problem with a MPD source is the lack of precipitation and thus potential for surface infiltration in this arid region. Assuming that Freeling Heights plateau is the catchment area (147 km^2; Sandiford et al., 1998a), an annual rainfall of 20.3 mm (BOM, 2001) and that all precipitation infiltrates the MPD and none is lost via evaporation, we calculate that the annual precipitation represent $3.83 * 10^{10}$ m^3/year, or 1.21 L/s. Therefore, the current precipitation levels are not capable of maintaining the present day discharge from the PHS. The high apparent variability of the flow rate over the observation period (73 years), together with the relatively short residence time for water through MPD, supports an origin of PHS water from the MPD. The low precipitation may explain why the PHS are the only hot springs in the region. By limiting convective heat transport, the low precipitation also increases the temperature of the thermal system; this can explain why other U-rich environments (e.g., Athabasca Basin, Northern Saskatchowan, Canada; Kotzer and Kyser, 1995) do not feature similar hot springs.

6.2. Modern water and fossil hydrothermal deposits

The geochemical similarity between the jasperoidal quartz outcrop and the water suggests that the PHS represent the surface expression of an epithermal mineralisation system at depth. Similarly, the high U content found in RC water suggest that it may be involved in U-mineralisation. In both cases, there are fossil deposits (Mt. Gee epithermal; Beverley U), which may have formed from waters with similar composition. In order to investigate possible relationship between fossil and modern groundwater, we used numerical modelling to simulate two possible mineralisation processes: cooling of PHS fluid, and reduction of RC fluid by biological matter and/or pyrite.

RC has the highest U concentration among sampled waters. Uranium is typically extracted from rocks by oxidising waters where insoluble U^{4+} in the rocks is converted to the soluble uranyl ($[UO_2]^{2+}$) ion; uranyl solubility is further increased by complexing with anions such as HCO_3^- and SO_4^{2-}. The lack of U in most sampled waters reflects reducing conditions unsuitable for U mobilization. The Eh measurements plot next to the uraninite solubility line (Fig. 5) and in this case most waters would have little capacity to transport U. This explains both the absence of U in Pool 1 and the increase in U downstream, as waters become more oxidizing and extract U from alluvial sediments.

Reaction paths were calculated for the reduction of RC water by carbon (Fig. 12a,b) and pyrite (Fig. 12c), using a simple titration method. The model shows that it would take as little as 10^{-8} g of carbon for pitchblende to precipitate from 1 kg of water (Fig. 12b). Uranium in roll-front deposits is usually associated with pyrite and V, Se and Mo minerals (Dahlkamp, 1993). In our simulation, V is represented by V_2O_3 (karelianite) and V_3O_5; Se occurs as Cu, Pb, Ag, Ni and Mo selenides and Mo in $MoSe_2$ (note that molybdenite is not included in the LLNL database). Channel or basal U-deposits often include sulphides of Cu, Fe, Mo, Pb, Zn, whereas U–V deposits often contain As-bearing minerals in trace amounts and occur close to barite cementation (Dahlkamp, 1993). The reaction path predicts that both Cu and Pb sulphides would precipitate as galena (PbS) and covellite (CuS). The presence of orpiment (As_2S_3) and witherite ($BaCO_3$) indicates that both barium and arsenic-bearing minerals may be associated with a U deposit formed from this water. The simulation in Fig. 12a was performed assuming that the dissolved silica concentration is controlled by quartz, whereas in Fig. 12b SiO_2(aq) is controlled by amorphous silica. Coffinite, the main U-carrier at the Beverley U-mine, becomes the stable U-mineral. Reaction with pyrite (Fig. 12c) produces a similar orebody. Palladium is predicted to precipitate early in all models; however, the RC water do not carry enough Pd to form a significant anomaly, and the predicted Pd concentrations are less than 10^{-10} gram per gram of uraninite/coffinite. High Pd concentrations associated with U have been reported from unconformity type U-deposits in the Alligator Rivers field in the Northern Territory, Australia (Mernagh et al., 1994) and the Athabasca basin of Canada (Wray et al., 1985). Mernagh et al. (1994) suggest that the ratio of PGE + Au to U in these deposits is controlled by the extent of the reduction: a rise in pH and a small degree of reduction are efficient precipitation mechanisms for PGE + Au, whereas U deposition requires a more

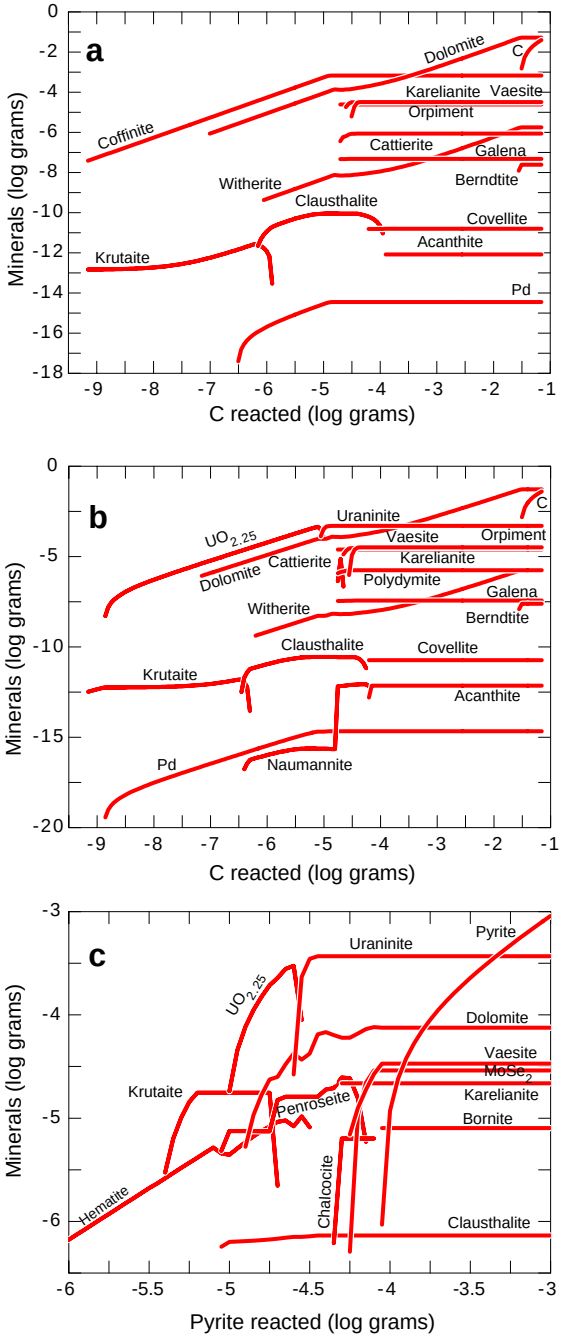

Fig. 12. Simulation of potential ore-forming processes involving Radium Creek Water. (a) Reaction with organic carbon-bearing quartzite, assuming that dissolved silica concentration is controlled by quartz; (b) Reaction with organic carbon-bearing quartzite, assuming that dissolved silica is controlled by SiO_2(am); (c) Reaction with pyrite-bearing quartzite, assuming that dissolved silica is controlled by quartz. Chemical formulae of unusual minerals: berndtite SnS_2; cattierite CoS_2; clausthalite PbSe; karelianite V_2O_3; krutaite $CuSe_2$; naumannite Ag_2Se; penroseite $NiSe_2$; polydymite Ni_3S_4; vaesite NiS_2; witherite $BaCO_3$.

extensive reduction. Our simulation predicts early Pd precipitation if uraninite is the stable U-mineral; however, coffinite precipitates before Pd if dissolve silica is controlled by SiO_2(am).

The average ore at Beverley contains 0.49 wt.% U and only low concentrations of As, V and Se (50, 50 and 6 ppm, respectively; Heathgate Resources, 1998). The predicted final ore composition for the simulation in Fig. 12a, for a similar U grade, has 219 ppm As and 188 ppm V (Se minerals are predicted to redissolve, and occur only at <1 ppm level in the simulated ore). Detailed on-going mineralogical studies have revealed the presence of Se (rare claustha-lite inclusions in uraninite/cofffinite) and V (as

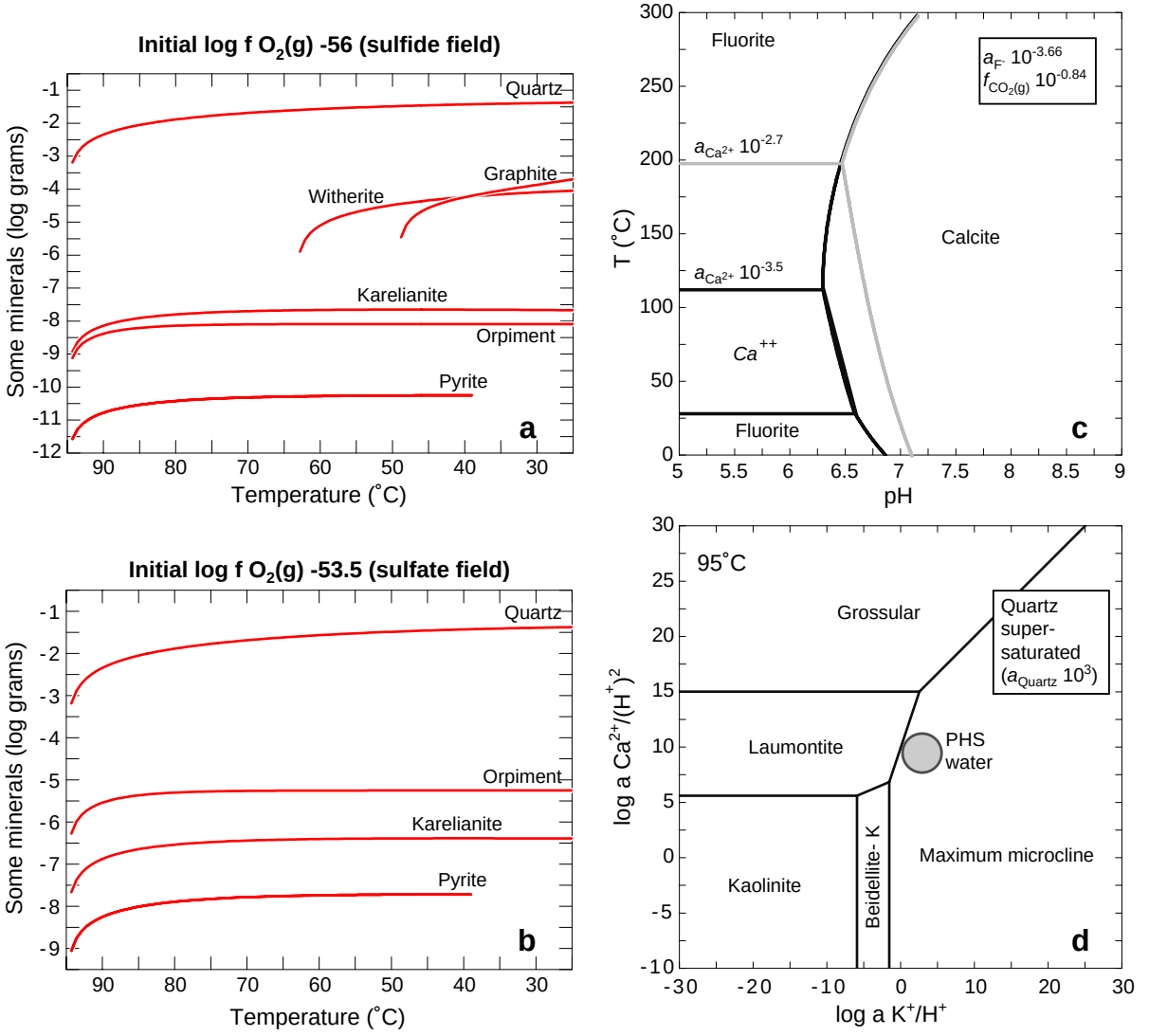

Fig. 13. Cooling of the Paralana Hot Springs fluid. (a) Mineral precipitation sequence, for starting redox conditions more reducing than the sulfide/sulfate buffer. (b) Mineral precipitation sequence, for starting redox conditions more oxidised than the sulfide/sulfate buffer. (c) Temperature-pH diagram illustrating the stability of fluorite and calcite with respect to the chemistry of the Paralana Hot Springs water. (d) Activity–activity diagram illustrating the stability of laumontite with respect to the Paralana Hot Springs water. Diagram drawn for high silica supersaturation (a Quartz=1000); prehnite and scolecite are the predicted stable zeolite phases at a Quartz <200.

carnotite) within the ore at Beverley (Wulser, oral communication, 2005).

The similarity between the mineral assemblage above and the mineral assemblage associated with "roll front" U-deposits suggests that waters from RC have the potential to produce a U-deposit. The simple calculations presented here show that these waters may also represent the waters from which the Beverley U-deposit formed. However, detailed understanding of the mineralogical and geochemical zoning within the Berverley deposits are required to evaluate whether RC-type groundwaters may have been involved in its formation.

Cooling is the most likely precipitation mechanism for PHS. Cooling paths calculated using different initial redox conditions near the sulphate/sulphide coexistence boundary are shown in Fig. 13a,b. Results are qualitatively similar, though the mineral ratios change, and whiterite + graphite appear under reducing conditions. A redox state close to the sulphate/sulphide buffer at depth is indicated by the presence of fresh pyrite in rocks and gypsum in vugs of the jasperoidal outcrop next to Pool 1 at PHS. The predicted mineral assemblage is dominated by quartz, with only minor sulphides (pyrite) and minerals such as orpiment and karelianite, which are expected in epithermal context. The occurrence of clinobisvanite ($BiVO_4$) as a supergene mineral in an epithermal gold mineralisation along the Paralana fault at Lively suggests that both Bi and V were in the epithermal fluids (Collier and Plimer, 2002) and, only 200 m north of the hot springs, silica breccia fault fill contains arsenian pyrite. Au would precipitate, but only in very small quantities due to its low concentration in the PHS fluid. Characteristic accessory phases in the Palaeozoic Mt. Gee epithermal system are fluorite, calcite and laumontite. These minerals could easily precipitate from the PHS water. Higher temperature or Ca concentrations would lead to fluorite precipitation, while a slight increase in pH would stabilize calcite (Fig. 13c). The PHS water composition also lies next to the stability field of laumontite (Fig. 13d). Laumontite has been reported from geothermal fields at temperatures generally lower than 220–230 °C in rocks of various compositions (Gianelli et al., 1998); the lowest temperature occurring hydrothermal laumontite was in a Na–Cl–SO_4 springs at 43–89 °C in California (McCulloh et al., 1981).

7. Conclusions

Analysis of water, gas and rock samples from the PHS and water samples of groundwater from the Mt. Painter Inlier enables the characterization of this hydrothermal system in terms of physio-chemical characteristics, fluid sources and flow paths, heat sources, and mineralisation potential.

The PHS water is near neutral and contains low levels of dissolved elements. The changes in the physical and chemical parameters downstream from the source of the springs can be attributed to a decrease in temperature, and to interaction (sorption; micro-nutrient) with the large amount of biomatter in Pool 2.

Water in the PHS differs from groundwater in the Mt. Painter Inlier in that it is ~30 °C warmer, contains less total dissolved solids and more CO_2(aq), denoting a different source or flow path for this spring. Oxygen and hydrogen stable isotopic ratios indicate the water in PHS has a meteoric origin. Low levels of dissolved elements, recent gypsum and opaline silica mineralisation, and the absence of a hot water–rock trend in the stable isotopic ratios suggest the PHS water has not reached high temperatures. This is confirmed by geothermometric calculations indicating a temperature of last equilibration for water–rock interaction of 95 ± 5 °C. High Rn and He concentrations at PHS indicate a localized radiogenic source. Radiogenic decay is likely to heat the water by enhancing the local geothermal gradients for MPD. Published geothermal gradients suggest circulation depths of 1.4 to 2.4 km.

The PHS water is of meteoritic origin and could be sourced from either the Mt. Painter Domain or GAB aquifers. The Na–Cl–HCO_3 water type of the PHS differs from GAB waters but is similar to water from the Willawortina Formation in the Lake Frome plains, which is recharged from the MPD. The MPD source is further confirmed by the variability of the fluid flow at PHS and the low temperature of last fluid–rock interaction, which suggest relatively short residence times and a link to the local irregular precipitations. The position of PHS along the Paralana fault and their chemical similarity suggest that the fault system acts as a conduit for fluids. Similarities in the major and trace elements chemistry, and their common location on the Paralana Fault, indicate a common origin for

Black Spring and PHS. Slight differences in chemical and isotopic compositions are probably related to minor differences in flow path and residence times.

The RC water naturally contains high U concentrations, and reactive transport simulation shows that this water could produce a Beverley-type deposit through reduction by organic matter and/or sulphides. The apparent lack of As, Cu, Co minerals at Beverley could, in this case, be explained by a non-complete reduction of the fluid. The PHS water carries little U; however, by cooling, it can produce mineralisation similar to the jaspers outcropping around Pool 1. It could also result in the deposition of "Mt. Gee" style mineralisation, especially if heating to ~200 °C would occur. The PHS water contains the Ba, Mo and F necessary to precipitate characteristic accessory minerals such as barite, fluorite and molybdenite. The Mt. Gee system also contains elevated U and REE concentrations, which cannot be produced by the PHS water. This hints to special conditions during the formation of this system. Elburg et al. (2003) propose a link between the epithermal mineralisation at Mt. Gee and the intrusion of the ~440 My British Empire granite. This link is also supported by magmatic isotopic signature for the sulphur in Mt. Gee sulphides (Lambert et al., 1982). Additional heat provided by the intrusion could explain the difference between the Mt. Gee system and the fault-bound jasperoidal mineralisation.

This study shows that the chemistry of modern groundwater in the MPD is closely related to that of fossil regional ore-forming fluids. The formation of economic and sub-economic mineral deposits depended on special circumstances that affect fluid flow and chemistry. For example, the Mt. Gee–Mt. Painter epithermal system may result from mantle heat input provided by the intrusion of the British Empire Granite. On the other hand, the Beverley style mineralisation could be linked to wetter climate (e.g., Tertiary), drawing large amounts of RC-type groundwater into the Lake Frome embayment.

Acknowledgements

We thank Michelle Carey for the IC analyses, John Tsiros for the ICP-MS analyses, Ian Cartwright and Ben Petrides for the stable isotope analyses of water and gas, David Stone of ANSTO for the gas analyses, Robert Douglass for preparing the thin sections, and Jim Cull for helping with the heat flow calculations. We are indebted to Kristen Byford, Josquin Tibbits, Edwin Byford, Stefan Ansermet, Ben McHenry, Michael Long and Barbara Etschmann for their help during field work. Special thanks are due to Doug Sprigg for offering hospitality at Arkaroola Wilderness Resort and for showing us the Northern Flinders Ranges from the air. This work benefited greatly from detailed and insightful comments by two anonymous reviewers. **[DR]**

References

AEA/WMO, 2004. Global Network of Isotopes in Precipitation. The GNIP Database. Accessible at: http://isohis.iaea.org. Isotopic Analyses for the Alice Springs station: Commonwealth Scientific and Industrial Research Organizations, Glen Osmond, South Australia, Australia.

Anderson, G.M., Crerar, D.A., 1993. Thermodynamics in Geochemistry. Oxford University Press, New York. 588 pp.

Anitori, R.P., Trott, C., Saul, D.J., Bergquist, P.L., Walter, M.R., 2002. A culture-independent survey of the bacterial community in a radon hot spring. Astrobiology 2, 255–270.

Arnorsson, S., 1975. Application of the silica geothermometer in low temperature hydrothermal areas in Iceland. American Journal of Science 275, 763–784.

Barnes, H.L., Rose, A.W., 1998. Origins of hydrothermal ores. Science 279, 2064–2065.

Bethke, C.M., 1998. The Geochemist's Workbench. Hydrogeology Program. University of Illinois, Illinois.

BOM, 2001. Climate Data from Arkaroola Weather Station. Bureau of Meteorology, Melbourne.

Clark, I.D., Fritz, P., 1997. Environmental Isotopes in Hydrogeology, 2nd ed. Lewis Publishers, New York.

Coats, R.P., Blissett, A.H., 1971. Regional and economic geology of the Mount Painter province Department of Mines. Geological Survey of South Australia, Bulletin 43 426 pp.

Collier, J., 2000. Geology and the Associated Mineralisation of the Arkaroola Creek Area, South Australia. Unpublished Honours Thesis, The University of Melbourne, Melbourne, 1–120 pp.

Collier, J.B., Plimer, I.R., 2002. Supergene clinobisvanite pseudomorphs after supergene dreyerite from Lively's Mine, Arkaroola, South Australia. Neues Jahrbuch fuer Mineralogie Monatshefte., 401–410.

Cox, R., Barron, A., 1998. Great Artesian Basin: Resource Study. Great Artesian Basin Consultative Council, Australia.

Cull, J.P., 1982. An appraisal of Australian heat-flow data. BMR Journal of Australian Geology and Geophysics 7, 11–21.

Cull, J.P., 1991. Heat flow and geophysics in Australia. In: Cermak, V., Rybach, L. (Eds.), Exploration of the Deep Continental

Crust: Terrestrial Heat Flow and Lithosphere Structure. Springer-Verlag, Germany, pp. 486–500.
Cull, J.P., Conley, D., 1983. Geothermal gradients and heat flow in Australian sedimentary basins. BMR Journal of Australian Geology and Geophysics 8, 329–337.
Dahlkamp, F.J., 1993. Uranium Ore Deposits. Springer-Verlag, Germany.
Deines, P., Langmuir, D., Harmon, R.S., 1974. Stable carbon isotope ratios and the existence of a gas phase in the evolution of carbonate groundwaters. Geochimica et Cosmochimica Acta 32, 657–660.
Domenico, P.A., Schwartz, F.W., 1998. Physical and Chemical Hydrogeology. John Wiley and Sons, Inc., New York.
Drever, J.I., 1997. The geochemistry of natural waters. Surface and Groundwater Environments. Prentice Hall, Upper Saddle River, NJ. 436 pp.
Drexel, J.F., Major, R.B., 1987. Geology of the uraniferous breccia near Mt. Painter, South Australia and revision of rock nomenclature. Geological Survey of South Australia, Quaterly Geological Notes 104.
Drexel, J.F., Major, R.B., 1990. Mount Painter uranium-rare earth deposits. In: Hughes, F.E. (Ed.), Geology of the Mineral Deposits of Australia and Papua New Guinea. Australasian Institute of Mining and Metallurgy, Melbourne, pp. 993–998.
Drexel, J.F., Preiss, W.V., Parker, A.J., 1993. The geology of South Australia. Volume 1: The Precambrian, Geological Survey of South Australia, Bulletin, vol. 54. 242 pp.
Druschel, G.K., Rosenberg, P.E., 2001. Non-magmatic fracture-controlled hydrothermal systems in the Idaho Batholith: south fork payette geothermal system. Chemical Geology 173, 271–291.
Eaton, A.D., Clesceri, L.S. and Greenberg, A.E. (Eds.), 1995. Standard Methods for the Examination of Water and Wastewater. American Public Health Association, American Water Works Association and the Water Environment Federation, USA. 19th edition.
Elburg, M., Bons, P., Foden, J., Brugger, J., 2003. A newly defined Late Ordovician magmatic-thermal event in the Mt. Painter Province, Northern Flinders Ranges, South Australia. Australian Journal of Earth Sciences 50, 611–631.
Evensen, N.M., Hamilton, P.J., O'Nions, R.K., 1978. Rare-earth abundances in chondritic meteorites. Geochimica et Cosmochimica Acta 42, 1199–1212.
Fetter, C.W., 1994. Applied Hydrogeology. Prentice Hall, New Jersey.
Foster, D.A., Murphy, J.M., Gleadow, J.W., 1994. Middle tertiary hydrothermal activity and uplift of the Northern Flinders Ranges, SA: insights from apatite fission track thermochronology. Australian Journal of Earth Sciences 41, 11–17.
Freeze, R.A., Cherry, J., 1979. Groundwater. Prentice-Hall Inc, New Jersey.
Gianelli, G., Mekuria, N., Battaglia, S., Chersicla, A., Garofalo, P., Ruggieri, G., Manganelli, M., Gabregziabher, Z., 1998. Water–rock interaction and hydrothermal mineral equilibria in the Tendaho geothermal system. Journal of Volcanology and Geothermal Research 86, 253–276.
Gonfiantini, R., 1986. Environmental isotopes in lake studies. In: Fritz, P., Fontes, J.C. (Eds.), Handbook of Environmental Isotope Geochemistry, The Terrestrial Environment, vol. 2. B. Elsevier, Amsterdam, pp. 113–168.
Grant, K., 1938. The radioactivity and composition of the water and gases of the Paralana Hot Spring. Transactions of the Royal Society of South Australia 62, 357–364.
GSSA, 1983. NATMAP Umberatana Map Sheet. Primary Industries and Resources South Australia, South Australia.
Habermehl, R., 1980. The great artesian basin, Australia. BMR Journal of Australian Geology and Geophysics 5, 9–38.
Habermehl, R., 1998a. Hydrogeology. In: Cox, R., Barron, A. (Eds.), Great Artesian Basin: Resource Study. Great Artesian Basin Consultative Council, Australia, pp. 44–60.
Habermehl, R., 1998b. Hydrogeology of the Great Artesian Basin. Australian Geological Survey Organisation, Australia.
Heathgate Resources, 1998. Beverley Uranium Mine: Environmental Impact Statement. Heathgate Resources Pty Ltd, South Australia.
Heinrich, C.A., Walshe, J.L., Harrold, B.P., 1996. Chemical mass transfer modelling of ore-forming hydrothermal systems— current practice and problems. Ore Geology Reviews 10, 319–338.
Henley, R.W., 1985. The geothermal framework for epithermal deposits. In: Berger, B.R., Bethke, P.M. (Eds.), Geology and Geochemistry of Epithermal Systems, Reviews in Economic Geology, vol. 2. The Economic Geology Publishing Company, El Paso, Texas, pp. 1–24.
Herczeg, A.L., Torgersen, T., Chivas, A.R., Habermehl, M.A., 1991. Geochemistry of ground waters from the Great Artesian Basin, Australia. Journal of Hydrology 126, 225–245.
Hillis, R., Hand, M., Mildren, S., Morton, J., Reid, P., Reynolds, S., 2004. Hot dry rock geothermal exploration in Australia. In: Boult, P.J., Johns, D.R., Lang, S.C. (Eds.), Eastern Australian Basins Symposium: II. Petroleum Exploration Society of Australia, Special Publication, pp. 413–421.
Hoefs, J., 1997. Stable Isotope Geochemistry. Springer Verlag. 201 pp.
Howard, L.E., Sass, J.H., 1964. Terrestrial heat flow in Australia. Journal of Geophysical Research 69, 1617–1626.
Howles, S.R., 2000. Beverley uranium project—groundwater resources, management and monitoring. MESA Journal 17, 4–6 (April).
Huttrer, G.W., 2001. The status of world geothermal power generation 1995–2000. Journal of the Japan Geothermal Energy Association 38, 27–45.
Idnurm, M., Heinrich, C.A., 1993. A palaeomagnetic study of hydrothermal activity and uranium mineralisation at Mt. Painter, South Australia. Australian Journal of Earth Sciences 40, 87–101.
Kakiuchi, M., Matsuo, S., 1979. Direct measurements of D/H and $^{18}O/^{16}O$ fractionation factors between vapor and liquid water in the temperature range from 10 to 40 °C. Geochemical Journal 13, 307–311.
Kerr, D.S., 1966. Hydrology of the Frome Embayment, vol. 27. SA Department of Mines, South Australia.
Kotzer, T.G., Kyser, T.K., 1995. Petrogenesis of the Proterozoic Athabasca Basin, Northern Saskatchewan, Canada, and its rela-

tion to diagenesis hydrothermal uranium mineralization and paleohydrogeology. Chemical Geology 120, 45–89.
Lambert, I.B., Drexel, J.F., Donnelly, T.H., Knuston, J., 1982. Origin of the breccias in the Mount Painter area, South Australia. Journal of the Geological Society of Australia 29, 115–125.
Lee, H.K., Uyedas, S., 1965. Review of heat flow data Chapter 6. Terrestrial Heat Flow, Geophysical Monograph, vol. 8, pp. 87–190.
Ludbrook, N.H., 1969. Tertiary period. In: Parkin, L.W. (Ed.), Handbook of South Australian Geology. Geological Survey of South Australia, Adelaide, pp. 172–203.
Mawson, D., 1927. The Paralana Hot Spring. Transactions of the Royal Society of South Australia 20, 391–397.
Mazor, E., Levitte, D., Truesdell, A.H., Healy, J., Nissenbaum, A., 1980. Mixing models and ionic geothermometers applied to warm (up to 60 °C) Springs: Jordan Rift Valley, Israel. Journal of Hydrology 45, 1–19.
McCulloh, T.H., Frizzell, V.A. Jr., Stewart, R.J., Barnes, I., 1981. Precipitation of laumontite with quartz, thenardite, and gypsum at Sespe hot springs, western Transverse Ranges, California. Clays Minerals 29, 353–364.
McKelson, J., 2000. Geology of the Paralana Hot Spring Area, North Flinders Ranges, South Australia. Unpublished Honours Thesis, The University of Melbourne, Melbourne, 1–120 pp.
McLaren, S., Dunlap, W.J., Sandiford, M., McDougall, I., 2002. Thermochronology of high heat-producing crust at Mount Painter, South Australia: implications for tectonic reactivation of continental interiors. Tectonics 21, 1275–1291.
Mernagh, T.P., Heinrich, C.A., Leckie, J.F., Carville, D.P., Gilbert, D.J., Valenta, R.K., Wyborn, L.A.I., 1994. Chemistry of low-temperature hydrothermal gold, platinum, and palladium (±Uranium) Mineralization At Coronation Hill, Northern-Territory, Australia. Economic Geology and the Bulletin of the Society of Economic Geologists 89, 1053–1073.
Mildren, S.D., Sandiford, M., 1995. Heat refraction and low-pressure metamorphism in the Northern Flinders Ranges, South Australia. Australian Journal of Earth Sciences 42, 241–247.
Mitchell, M.M., Kohn, B.P., O'Sullivan, P.B., Hartley, M.J., Foster, D.A., 2002. Low-temperature thermochronology of the Mt. Painter Province, South Australia. Australian Journal of Earth Sciences 49, 551–563.
Neumann, N., Sandiford, M., Foden, J., 2000. Regional geochemistry and continental heat flow: implications for the origin of the South Australian heat flow anomaly. Earth and Planetary Science Letters 183, 107–120.
Oxtoby, D.W., Nachtrieb, N.H., 1996. Principles of Modern Chemistry. Saunders College Publishing, Chicago.
Paul, E., Flöttmann, T., Sandiford, M., 1999. Structural geometry and controls on basement-involved deformation in the Northern Flinders Ranges, Adelaide Fold Belt, South Australia. Australian Journal of Earth Sciences 46, 343–354.
Polak, E.J., Horsfall, C.L., 1979. Geothermal gradients in the great Artesian Basin, Australia. Bulletin of the Australian Society of Exploration Geophysics 10, 144–147.
Pollack, H.N., Hurter, S.J., Johnson, J.R., 1993. Heat flow from the Earth's interior: analysis of the global data set. Reviews of Geophysics 31, 267–280.
Preiss, W.V., 1989. A stratigraphic and tectonic overview of the Adelaide Geosyncline, South Australia. In: Jago, J.B., Moore, P.S. (Eds.), Special Publication 16: The Evolution of a Late Precambrian Early Palaeozoic Rift Complex: The Adelaide Geosyncline. Geological Society of Australia, Sydney, pp. 1–34.
Preiss, W.V., 1990. A stratigraphic and tectonic overview of the Adelaide Geosyncline, South Australia. In: Jago, J.B., Moore, P.S. (Eds.), The Evolution of a Late Precambrian–Early Palaeozoic Rift Complex: The Adelaide Geosyncline, Geological Society of Australia, Special Publication, vol. 16. Watson, Ferguson and Company, Brisbane, pp. 1–33.
Preiss, W.V., 1993. Delamerian fold belt. In: Drexel, J.F., Preiss, W.V., Parker, A.J. (Eds.), Bulletin 54: The Geology of South Australia. Mines and Energy Geological Survey of South Australia, South Australia, pp. 23–24.
Roy, R.F., Beck, A.E., Touloukian, Y.S., 1981. Thermophysical properties of rocks. In: Touloukian, Y.S., Rudd, W.R., Roy, R.F. (Eds.), Physical Properties of Rocks and Minerals. McGraw-Hill, New York.
Sandiford, M., Hand, M., McLaren, S., 1998a. High geothermal gradient metamorphism during thermal subsidence. Earth and Planetary Science Letters 163, 149–165.
Sandiford, M., Paul, E., Flöttmann, T., 1998b. Sedimentary thickness variations and deformation intensity during basin inversion in the Flinders Ranges, South Australia. Journal of Structural Geology 20, 1721–1731.
Sheard, M.J., Smith, P.C., 1995. Karst and mound spring deposits. In: Drexel, J.F., Preiss, W.V. (Eds.), The Geology of South Australia: The Phanerozoic. Mines and Energy Geological Survey of South Australia, South Australia, pp. 257–260.
Sprigg, R.C., 1984. Arkaroola—Mount Painter in the Northern Flinders Ranges, S.A.: The Last Billion Years. Arkaroola Pty Ltd, Australia.
Stamoulis, V., Hore, S., Preiss, W.V., Conor, C.H.H., 1999. Mt. Painter Mt. Babbage Inlier Curnamona Craton: LANDSAT image. Primary Industries and Resources South Australia, South Australia.
Teale, G.S., 1993. Mount Painter and Mount Babbage Inliers. In: Drexel, J.F., Preiss, W.V, Parker, A.J. (Eds.), Bulletin 54: The Geology of South Australia, Mines and Energy Geological Survey of South Australia, pp. 93–100. South Australia.
van Middlesworth, P.E., Wood, S.A., 1998. The aqueous geochemistry of the rare earth elements and yttrium: Part 7. REE, Th and U contents in thermal springs associated with the Idaho batholith. Applied Geochemistry 13, 861–884.
Walker, S., 1999. Beverley Uranium Project—in situ mining approved. MESA Journal 13, 8–10.
Wray, E.M., Ayres, D.E., Ibrahim, H., 1985. Geology of the Midwest uranium deposit, Northern Saskatchewan. Canadian Institute of Mining and Metallurgy 32, 54–66.